Precision microvertex detectors

N. M. Nikityuk
Joint Institute for Nuclear Research, Dubna

Fiz. Élem. Chastits At. Yadra **28**, 191–242 (January–February 1997)

The current status and future perspectives of the development of high-precision microvertex detectors are reviewed. A description is given of the characteristics, operating principles, and methods of signal readout from microvertex detectors designed on the basis of semiconductor technology and fiber-optics light-guide techniques. The parameters of the best known microvertex detectors used in fixed-target and collider experiments are given in tables. The specialized processors used for fast calculation of the impact parameter and selection of events containing decay vertices are discussed. © *1997 American Institute of Physics*. [S1063-7796(97)00501-9]

INTRODUCTION

Semiconductor detectors have existed for more than 40 years. In a pioneering study in 1951 (Ref. 1), it was shown that α particles passing through a reverse-biased p–n junction in germanium generate a noticeable signal. This in fact is the basic principle upon which all modern semiconductor detectors are based. However, as noted in Ref. 2, until the end of the 1970s semiconductor detectors were used to measure the energy of particles passing through them. With few exceptions, high-energy physics experiments have used silicon detectors, owing to the fact that they can operate at room temperature. Such detectors are fabricated using modern technology on the basis of high-resistivity silicon (resistivity of the order of several KΩ/cm). Subsequent research directed to improving the resolution of track detectors led to the development of microstrip semiconductor detectors. Here we shall briefly review the studies devoted to semiconductor detectors and their use.

The literature on semiconductor detectors from 1951 up to the end of the 1970s is reviewed in Ref. 3. According to the classification of Ref. 4, semiconductor detectors can be divided into two groups. (1) Classical detectors like photodiodes, x-ray detectors, semiconductor counters, microstrip detectors, and also certain types of pixel detectors. (2) Memory detectors like CCD matrices, silicon drift chambers, and pixel detectors with storage elements.

In this review we shall discuss the use of semiconductor counters, microstrip detectors, and CCD matrices as vertex detectors. All of these are widely used in experiments. Compared to gas-based detectors, silicon semiconductor microstrip detectors are an order of magnitude more accurate and are very fast. Their preparation is based on well developed planar technology (accuracy better than 1 μm), so that hundreds of recording channels can exist on a single crystal. The physics and technology of silicon semiconductor detectors are reviewed in detail in Ref. 5, which also describes the various types of these detectors. The typical structure, geometrical dimensions, and electrode geometry of one of the first microstrip detectors are shown in Fig. 1 (Ref. 6). It is made from a fully depleted silicon crystal with a diode structure and a high resistivity >10 kΩ/cm. One side of the crystal surface is divided into conducting strips of pitch 20–50 μm, which are used for charge collection. The typical electron collection time is 4 nsec. The signals are read out from each microstrip, or from groups of strips connected together in some manner. The charge-division method is widely used to improve the accuracy of recording event coordinates and to decrease the number of amplifiers needed. The use of this technique allows the interpolation method to be used for calculating the coordinates of a charged particle. In more elaborate microstrip detectors it is possible to read out the signals from opposite sides of the detector.[7] It should be noted that silicon detectors do not have internal signal amplification, so that there are strong requirements on the recording electronics, particularly regarding noise stability.

Semiconductor counters. Semiconductor counters are used as active targets. In the NA14 experiment at CERN,[8] the first version of the target consisted of 43 thin ($300\times100\times100$ μm) wafers with 200 μm spacing between them. The small target dimensions allow events to be recorded with high accuracy. The track reconstruction is done by analyzing the ionization loss in different counters of the target. The measured lifetime of the charmed meson was 9.5×10^{-13} sec. To increase the sensitivity to particles with shorter lifetime, a combination target was built. This consists of a miniature germanium target and a telescope made of thin silicon counters.[9] To decrease the input capacitance, the silicon counters are divided into sectors. The use of the germanium target allowed the sensitivity in the region of the primary decay vertex to be increased by a factor of 2.5. Active targets are used especially effectively in combination with microstrip detectors. The main drawback of active silicon detectors is the difficulty of identifying multiparticle processes. In addition to semiconductor detectors and CCD matrices, precision microvertex detectors are also constructed using microstrip gas detectors and detectors based on scintillating fiber-optics light guides (SCIFI detectors).

Our goal in this review is to describe briefly the current status of the techniques and perspectives for future development in use of precision vertex detectors. After the Introduction, the first three sections are devoted to semiconductor microvertex detectors. In Sec. 1 we discuss the parameters and methods of constructing precision vertex detectors for fixed-target experiments. Section 2 contains a description of the specialized processors used to reconstruct decay vertices. In Sec. 3 we discuss the construction and parameters of precision vertex detectors designed for collider experiments.

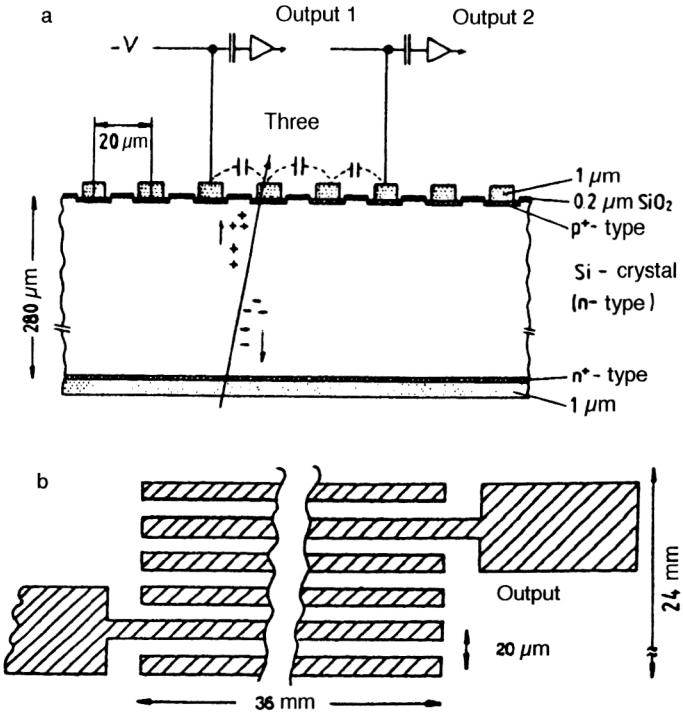

FIG. 1. (a) Structure of the microstrip semiconductor detector; (b) microstrip geometry.

The electronics of microvertex detectors is discussed in Sec. 4. Section 5 is devoted to the use of microstrip gas detectors in the construction of microvertex detectors and, in particular, for the future CMS detector. Pixel detectors are discussed in Secs. 6 and 7. In Sec. 8 we discuss the use of fiber-optics light guides in the construction of microvertex detectors.

1. SEMICONDUCTOR MICROSTRIP MICROVERTEX DETECTORS FOR FIXED-TARGET EXPERIMENTS

As noted in Ref. 10, in the study of the physics of beautiful particles, fixed-target experiments have certain advantages over collider experiments. These are: (1) Beautiful particles scatter from the target in the forward direction, where the detector is located; (2) it is simpler to reconstruct the primary decay vertex. Microstrip detectors were first used experimentally in the 1980s in fixed-target experiments. Here we shall discuss the characteristics of the best-known precision detectors used in fixed-target experiments.

The microvertex detector for the ACCMOR spectrometer. A microvertex detector used to obtain a resolution of 5 μm and a two-track resolution of 60 μm is described in Ref. 10. The detector consists of a beam telescope and an active target. The beam telescope contains six microstrip planes. The strips in the first four planes have a pitch of 50 μm and are arranged horizontally and connected in pairs. The microstrips with pitch 20 μm in the other planes are inclined relative to the horizontal at angles of $\pm 14°$. The telescope is used to determine the location of a 200-GeV π^- beam. The active target consists of ten detectors of thickness 280 μm located at a distance of 500 μm from each other. Behind the target are several detectors with spacing of 400 μm, which are used to generate the trigger pulse. The vertex telescope (active target) consists of six detectors of thickness 280 μm and active area 24×30 mm^2. The signals recorded from the vertex telescope are read out by the economical charge-division method and are used to measure the impact parameter with record-setting resolution. This detector has been used to record 4×10^6 events which may contain charmed particles.

The microstrip vertex detector for the E687 experiment. This detector was designed to measure the lifetime of heavy beautiful particles in a photoproduction experiment at the Fermilab accelerator.[11] It allows the topology of such events to be reconstructed and the decay vertices to be identified. In Fig. 2 we show a diagram of the microvertex detector, which consists of a germanium target containing 40 microstrips and 12 microstrip silicon planes with signal readout possible from each microstrip. The microstrip backing is 300 μm thick and has area 5×5 cm^2. The parameters of individual groups of microstrip detectors are given in Table I. The first three detectors in each group give the X, Y, and U coordinates. The X, Y, and U planes are rotated relative to the horizontal plane by $-45°$, $-135°$, and $-90°$, respectively. In addition to events involving beautiful particles, this telescope has been used to record over a million events involving charmed particles.

The accuracy of the positioning of the detector planes is 3 μm. Of particular interest is the design of the trigger system (Fig. 3). With the goal of simplification, a simple algorithm is used which allows the presence of at least one decay vertex to be found in a recorded event. After storage of the signals in the trigger registers, the data from the leading plane are written into the register associated with the second plane. Then majority coincidence schemes are used to determine the presence of a decay vertex.

The microstrip detector for the Beatrice experiment (WA92). This detector was designed for experiments involv-

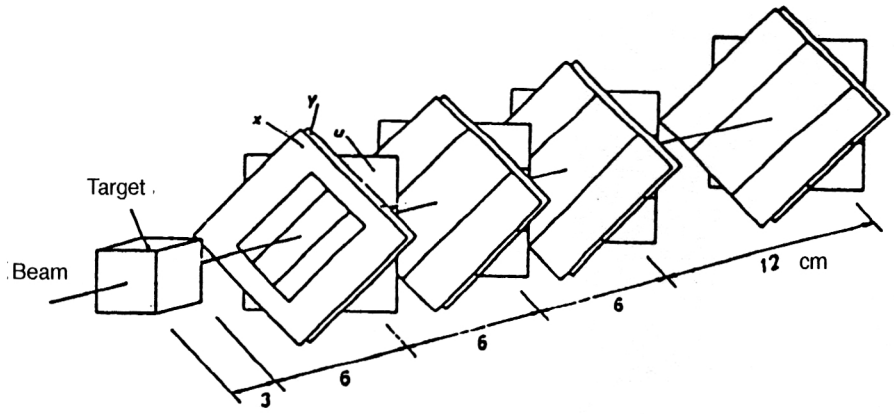

FIG. 2. Schematic diagram of the E687 telescope.

ing beautiful particles at CERN.[10] It allows the accurate reconstruction of events involving B decays. The detector consists of 16 microstrip planes with 10 μm pitch. The total thickness of the planes along the axis is 3.2 cm. The first 13 are Z planes located near the target. Of these, six detectors have a thickness of 150 μm, and the other planes have a thickness of 300 μm each. The 14th (Y) plane is rotated by 90° relative to the preceding planes. Planes 15 and 16 (U and V) are rotated by 10° and 14°. A record-setting spatial resolution of 3 μm has been obtained using this telescope. In Fig. 4 we give a general view of the detector, mounted on a ceramic backing. An efficient processor has been designed for this experiment. It will be described in the next section.

2. TRIGGER SYSTEMS FOR VERTEX DETECTORS

The authors of Ref. 12 describe an original algorithm for the selection of events with charmed particles. It uses both hardware and software methods of filtering complex events. The algorithm amounts to the following. Microstrip detectors are arranged in space in such a way that the ratio of the strip width and the distance from the target to a point between adjacent microstrips is a constant. Then all tracks originating at the point O, where the primary interaction vertex is located, satisfy the condition

$$n(a)=n(b)=n(c),$$

where n is the number of the triggered microstrip (Fig. 5). If the track does not "look" at the point O, within the error we have

$$n(a')\neq n(b')\neq n(c').$$

TABLE I. Parameters of the E687 microstrip detector.

Group number	1	2, 3 and 4
Total active area	2.5×3.5 cm^2	5×5 cm^2
Total number of microstrips (1+2+3+4)		8400
Central region:		
area	1×3.5 cm^2	2×5 cm^2
pitch	25 μm	50 μm
Outer regions:		
area	0.75×305 cm^2	1.5×5 cm^2
pitch	50 μm	100 μm

In practice, this means that after the event is recorded in memory, it is sufficient to erase all coordinates having the same address pertaining to the first three detectors. The remaining data can then be used to calculate the value of the impact parameter and to reconstruct the particle tracks. Since part of the information in this trigger system is processed by software, a better event-selection rate can be hoped for. The authors of Ref. 13 describe a high-speed trigger system which selects events containing secondary decay vertices in 10 μsec. This system uses a two-dimensional track processor developed for the DELPHI setup and described in detail in Ref. 14. The algorithm for the operation of the trigger system is essentially an improved version of the algorithm described above. It amounts to the following (Fig. 6). We use (X_v,Y_v) to denote the vertex coordinates and $(X_i,Z_i^{(j)})$ to denote the coordinates of tracks recorded by microstrip detectors: X_i ($i=1,2,\ldots,6$ is the number of detectors) is the position of the ith microstrip detector and $Z_i^{(j)}$ is the jth coordinate of the detector. Then in the XZ plane (Fig. 6a) the equation of a straight track will have the form

$$Z=bX+Z_v+h, \tag{1}$$

where Z_v is the Z coordinate of the vertex and h is the impact parameter, which is zero for all tracks originating at the primary decay vertex. The track reconstruction is carried out in four stages.

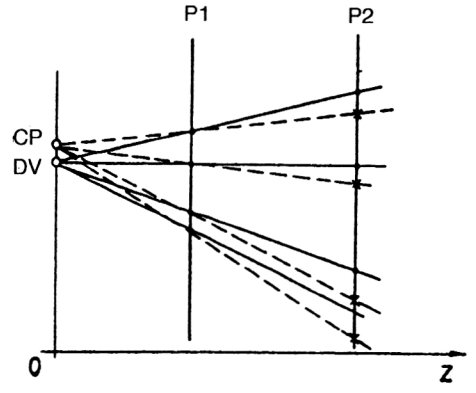

FIG. 3. Algorithm for the operation of a simple trigger. P1 and P2 are the detector planes, CP is the projection center, and DV is the decay vertex.

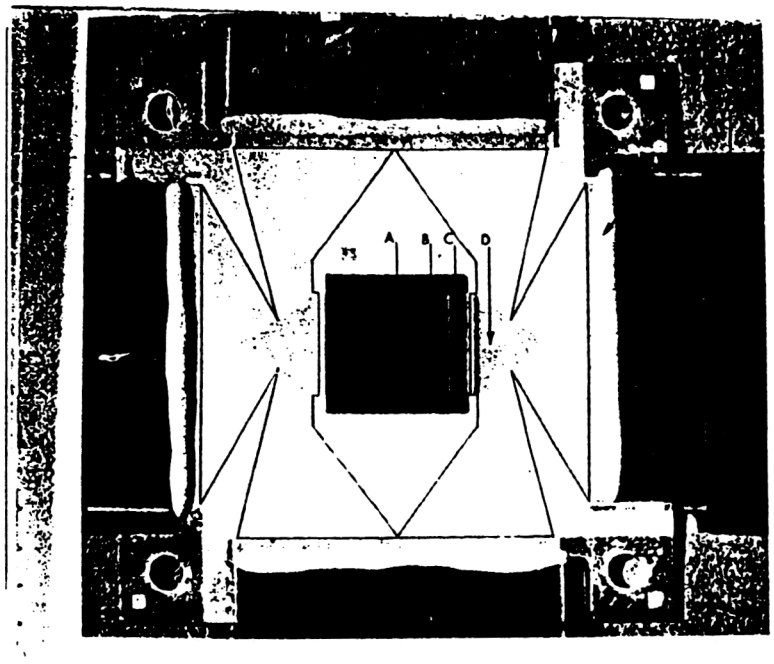

FIG. 4. General view of the microvertex detector. A is the active region, B are printed leads, C are leads connecting the microstrips to the ceramic backing, D are leads located on the ceramic, E are connections between the ceramic backing and the flexible cable, and F is the connection between the ceramic backing and the electronic readout system.

Step 1. Transformation of the coordinates. All points $(X_i, Z_i^{(j)})$ undergo a transformation of the type

$$Z_i^{(j)} = \frac{X_6}{X_i}(Z_i^{(j)} - Z_v). \tag{2}$$

Then Eq. (1) can be written as

$$Z = Z_6^{(j)} - Z_v + h\frac{X_6 - X}{X} = Z_6^{(j)} + h\frac{X_6 - X}{X}. \tag{3}$$

It should be noted that the transformation (2) transforms straight tracks, for which the impact parameter is $h=0$, into parallel lines (see Fig. 6b), while tracks pertaining to secondary interaction vertices become hyperbolas.

Step 2. As follows from (3), primary tracks each have six points with equal abscissas, so that these coordinates, which are written in memory, are erased, thereby simplifying the calculation of the impact parameter.

Step 3. A shift is performed, and the impact parameter is determined. To all $Z_i^{(i)}$ we add the quantity

$$n_i(h)w = h\frac{X_i - X_6}{X}, \tag{4}$$

where w is the pitch of the microstrip detector and n_i is the h-dependent number which best approximates Eq. (4). After this transformation, tracks having nonzero impact parameter reduce to a constant function of X. After these tracks are found, it is possible to calculate the value of the impact parameter by counting the number of shifts in the first detector:

$$h_1 = n_1(25\ \mu\text{m})\frac{X_1}{X_1 - X_6}.$$

Step 4. The coordinates of the corresponding decay vertices are found. As noted above, the event topology is reconstructed using a fast hardware programmable processor,

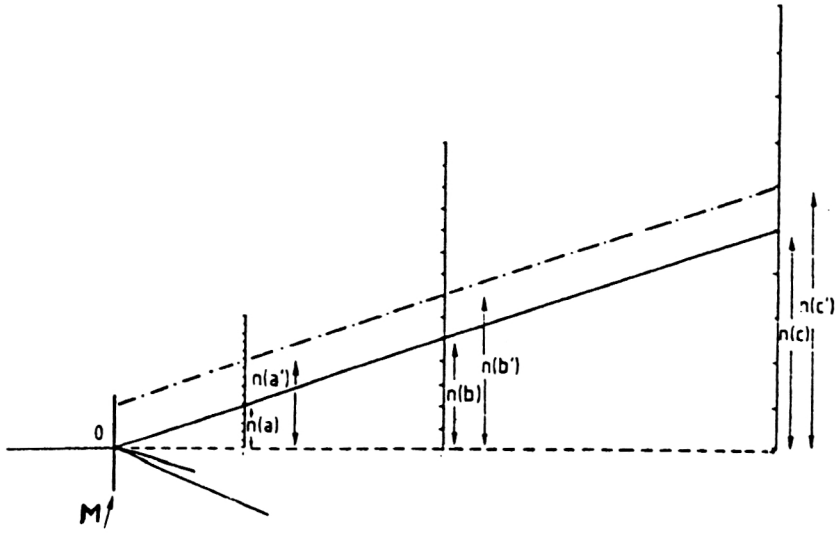

FIG. 5. Telescope used for generating the trigger in the WA82 experiment. T is the target, and n(a), n(b), and n(c) are the detector planes.

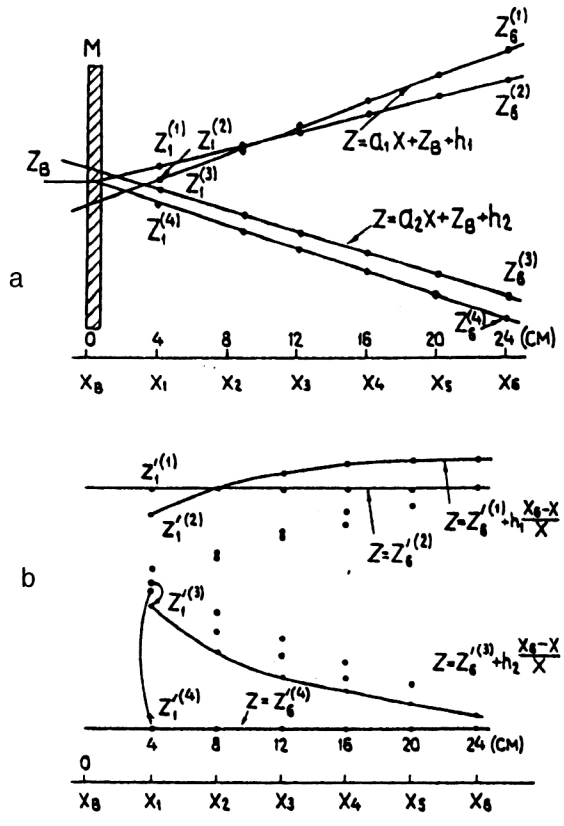

FIG. 6. (a) An example of an event with two primary decay vertices. (b) The same event after transformation.

whose operation is based on the contiguity-mask algorithm.[15] The algorithm is explained in Fig. 7. The data from the detectors are stored in trigger registers. The programmable memory in the first approximation is a matrix consisting of horizontal and vertical switches which are closed by the triggers of the registers in which ones are written. A modernized version of the specialized processor used in the WA92 experiment is described in more detail in Ref. 16.

The use of associative memory and analog neural networks. A trigger system designed for fast selection of events

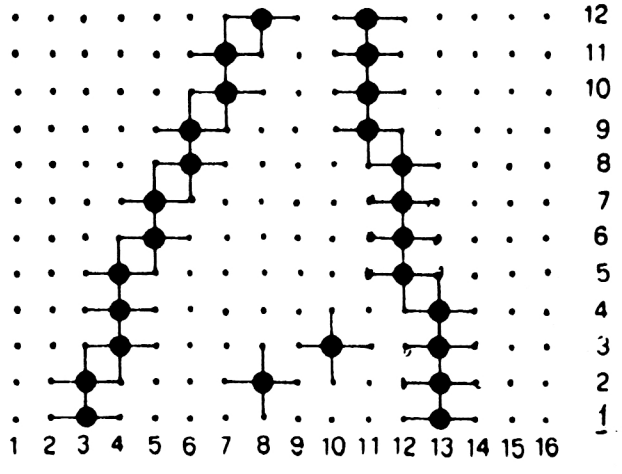

FIG. 7. The contiguity-mask algorithm.

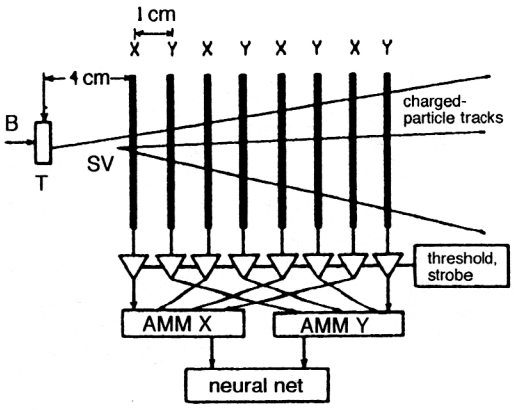

FIG. 8. Block diagram of the vertex detector. AMM is an associative memory module, B is the beam, SV is a secondary decay vertex, and T is the target.

involving heavy colored quarks incorporates associative memory modules containing 4096 cells in each module.[17] A more modern version of the trigger system uses an analog neural network.[18] It is necessary to use such complicated processors because finding a secondary decay vertex even off-line is a very complicated task. In Fig. 8 we show a block diagram of the microvertex detector. It consists of the target M, eight microstrip detectors rotated by 90° relative to each other, an electronic readout system, associative memory modules (AMM), and an analog neural network. Secondary decay vertices are sought in two steps. In the first, data on the most probable useful events are stored preliminarily in the AMM modules. These data might be, for example, the number of tracks in an event, the track slopes, and so on. In addition, it is known from general considerations that tracks (in an ideal situation) originating at a primary decay vertex appear as a set of points on a horizontal line, while secondary decay vertices appear as a set of points on a sloping line which intersects this horizontal line. After the data are recorded, a parallel search for tracks is conducted using the AMMs in the course of a few microseconds. If the search is successful, the data are sent to the inputs of the analog neural network.

The analog neural network is a VLSI chip designed by Intel. It has 64 inputs, 64 neural elements in a hidden layer, and 64 outputs. To enable the direct use of the neural network in an experiment, a hybrid processor was designed in the VME standard. It is shown schematically in Fig. 9. A 68070 CPU, an 80170 analog neural network, memory modules, and the corresponding interfaces are located on a board. The board also contains ADC and DAC modules for data exchange between processors. The entire hybrid processor is controlled by means of a personal computer. One of the awkward procedures associated with the use of a neural network is the need to train it by a special program. The use of the analog neural network has allowed a significant improvement in the selection of useful events.

3. VERTEX DETECTORS DESIGNED FOR COLLIDER EXPERIMENTS

Vertex detectors designed for collider experiments have a unique configuration in the form of a cylinder, with the

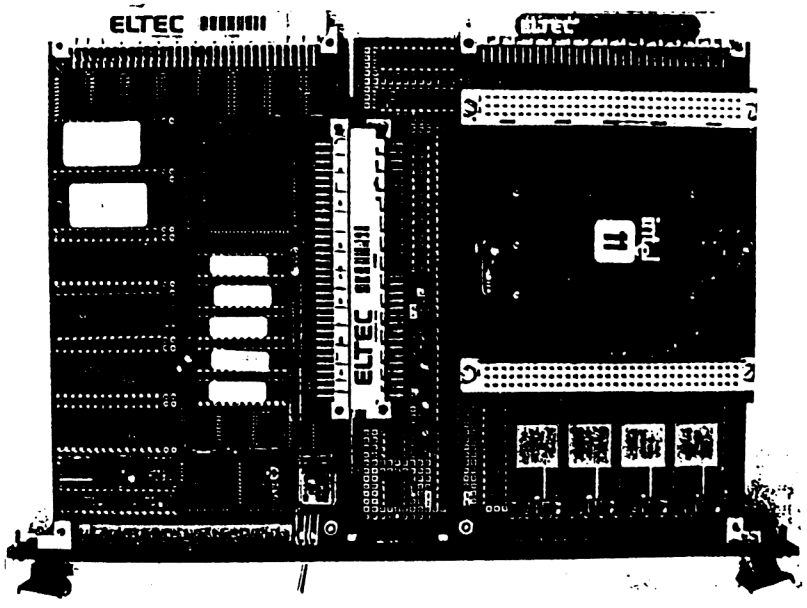

FIG. 9. Photograph of the VME module with an analog neural network.

beam pipe passing through the center (Fig. 10). They also have a more complicated mechanical construction and a larger number of detection channels (of the order of 10^5). To improve the accuracy of recording decay-vertex coordinates, a typical detector has several layers covered with microstrip detectors or other types of semiconductor detector. For a simplified detector design consisting of two layers located at distances L_1 and L_2 from the decay point with individual resolutions σ_1 and σ_2, the resolution of the impact parameter σ_i can be calculated from the expression[19]

$$\sigma_i^2=\sigma_1^2+R^2\alpha_{\rm ms}+R^2\alpha_{\rm track},$$

where σ_1 is the spatial resolution of the nearest detector plane, R is the distance from the first detector plane to the center of the beam, $\alpha_{\rm ms}$ reflects the effect of multiple scattering, and $\alpha_{\rm track}$ is the angular accuracy of the tracking system. For simplification, the material of the beam pipe is treated as a part of the inner layer of the detector. The main requirements on vertex detectors designed for LHC experiments are the following: (1) the accuracy of the inner detector (the one closest to the beam pipe) must be very high (on the order of several microns); (2) the amount of material in the detector and the beam pipe should be minimal; (3) the angular resolution of the entire tracking system should be of order 100 μrad.

A brief description of the vertex detector designed for the ATLAS collaboration together with its parameters is given in Ref. 19. The question of using two-coordinate (pixel) detectors for the inner layers of the vertex detector is discussed. The construction and parameters of the best-known microstrip detectors and electronic data readout and recording systems are described in Ref. 20. In Table II we list the setups designed for collider experiments. Most of these detectors are already being used in experiments.

More details about the detectors can be found in the corresponding references. Here we shall describe the best known microvertex detectors.

The Mark II microvertex detector. The Mark II microvertex detector was proposed for an experiment in 1985 at the SLAC linear collider and was first used in 1990 (Ref. 21). Before this, the lifetime of the $\tau^{\pm}$ leptons and the average lifetime of B hadrons were measured by using vertex drift chambers. In addition to raising the accuracy of measuring particle coordinates to 5 μm, as expected, the use of

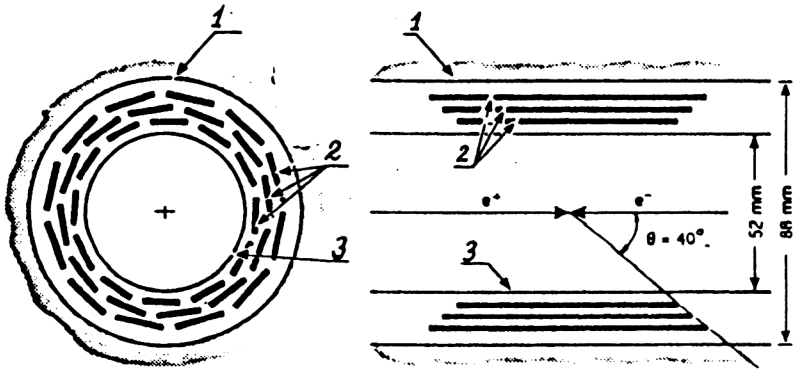

FIG. 10. Schematic diagram of the Mark II vertex detector with the beam pipe. (*1*) Inner wall of the vertex drift chamber; (*2*) silicon detectors; (*3*) ion lead.

TABLE II. Microstrip vertex detectors (Ref. 20).

Experiment	Collider	$\sqrt{s}$, GeV
MARK II	SLC (e^+e^-)	$94/Z^0$
DELPHI	LEP (e^+e^-)	$94/Z^0$
ALEPH	LEP (e^+e^-)	$94/Z^0$
OPAL	LEP (e^+e^-)	$94/Z^0$
CDF	TEVATRON ($p\bar{p}$)	1800
L3	LEP (e^+e^-)	$94/Z^0$
ARGUS	DORIS-II (e^+e^-)	$10/\Upsilon(4S)$
CLEO-II	CESR (e^+e^-)	$10/\Upsilon(4S)$
KEDR	VEPP-4 (e^+e^-)	$10/\Upsilon(4S)$

Note: Z^0, (4S)-particles.

the microvertex detector also allows an order of magnitude increase in the accuracy of measuring the impact parameter and improvement of the important two-track resolution to 5 mrad. The detector is shown schematically in Fig. 10. It consists of three concentric cylindrical surfaces, on which are mounted 36 modules (ladders) with one-sided readout. Special attention was paid to accurate alignment of the vertex detector and its individual parts. A three-dimensional microscope was used to obtain an accuracy of 40 μm. The collimated beam of an x-ray pipe was used to orient the microstrip detectors with an accuracy of 2 μm. In addition, capacitative sensors were used to detect changes in capacitance between the sensors and electrically grounded pads in order to monitor relative displacements of the vertex detector and the surrounding vertex drift chamber. Each detector (module) contains 512 microstrips with variable pitch: 25, 29, and 33 μm for the inner, middle, and outer layers, respectively. The strip length is also variable, so that the range of polar angle covered by the detectors can be as much as 40°. The microstrips are oriented parallel to the beam (the z axis), which allows measurement of the coordinates in the $r\phi$ plane. In Fig. 11 we give an overall view of a single module of the microstrip detector. Each module consists of a microstrip detector and two microcircuits H1 and H2, realized by hybrid technology. These devices effect the signal transfer from the microstrips to the inputs of the readout amplifiers. In turn, two pairs of large 128-channel Microplex VLSI chips are associated with each detector (see Table III). These chips ensure the amplification and readout of signals from the 18 432 microstrips. In Fig. 12 we show a photograph of the display of a two-jet Z^0 decay reconstructed by using the Mark II microvertex detector. The tracks of charged particles passing through the detector are shown as straight lines leaving the interaction point.

The DELPHI microvertex detector. The DELPHI detector is one of four universal setups used at the LEP accelerator and designed for the study of e^+e^- interactions at energies near the Z^0 mass. About 130 000 hadron events were recorded in 1990, and twice as many in 1991. Two modifications of vertex detectors were used in the DELPHI installation.[22] The detector installed in the LEP beam in 1989 consists of two concentric planes of radii 9.0 and 11 cm, on which microstrip detectors are mounted. Similar detectors had been used earlier in a fixed-target experiment. Microstrip detectors with a pitch of 25 μm are arranged parallel to the beam and the magnetic field. Each plane contains 24 modules, each of which in turn consists of four microstrip detectors. The vertex detector covers an angle of $\pm 45°$ and contains 165 886 microstrips altogether. Difficulties arise because one-dimensional detectors with signal readout from only a single plane are used. In an improved version of the microstrip detector the microstrip pitch is 16.6 μm, which allowed a high spatial resolution of order 5 μm and a two-track resolution of 100 μm to be obtained.

The decrease of the beam-pipe radius in 1991 allowed the installation of an additional inner cylinder of radius 6.3 cm over a distance of 24 cm. Since the radii of the concentric planes are different, the active length of the modules of the vertex detector is also variable and ranges from 1.92 to 3.20 cm. The characteristics of the final version of the detector are described in Ref. 22. In Fig. 13 we show a general view of one half of the microvertex detector. The use of a third plane allows measurement of the particle coordinates directly at the beam pipe. It was possible to decrease the error in determining the impact parameter from

$$((80\ \mu\text{m})^2+(120\ \mu\text{m}/p_t)^2)^{1/2}$$

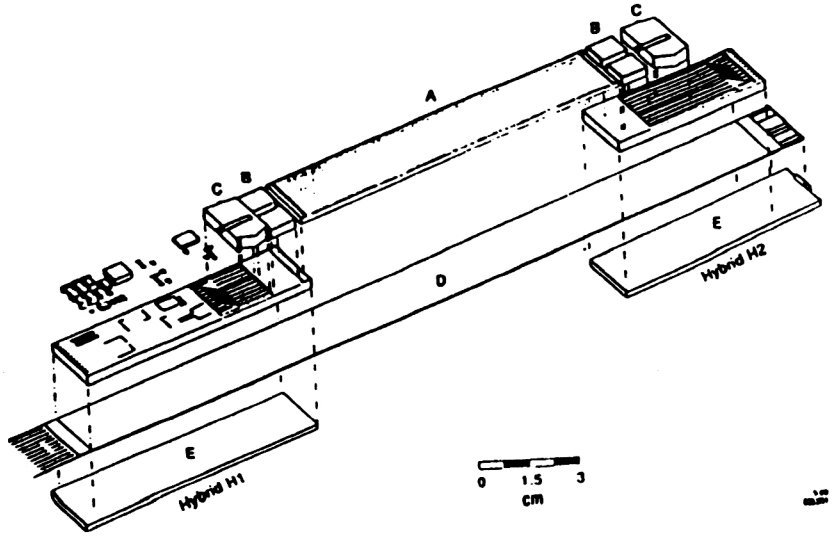

FIG. 11. General view of a microstrip module. A are microstrips, B are Microplex readout chips, C are buffer blocks, and D is a thin cable, and E are steel supports.

TABLE III. Parameters of semiconductor microstrip detectors.

	MARK II	DELPHI	ALEPH	OPAL	L3
Reference	21	22	23–26	27–28	29–31
Number of layers	3	3	2	2	2
Radii, cm					
r_1	2.9	6.3	6.3	6.2	6.1
r_2	3.4	9.0	-	-	-
r_3	3.8	11.0	10.7	7.7	7.8
Angle covered, %					
	0.65	0.86	0.87	0.82	0.92
	0.65	0.80	-	-	-
	0.65	0.73	0.75	0.76	0.88
Surface overlap, %	-	14	4	-	12
Number of detectors	36	288	96	75	96
Silicon area, m^2	0.05	0.42	0.25	0.15	0.30
Number of VLSI chip readouts	144	576	1152	125	576
Number of readout channels	18432	73728	73728	16000	73728
Signal-to-noise ratio	18	14	17	22	-
Individual resolution, μm	7	7–9	12($r\phi$) 12(rz)	5	7($\bar{r}\phi$) 14(rZ)
Impact parameter, μm	25±5		15, $r\phi$ 25, rz	-	-

Note: – No information.

to

$$(24\ \mu\text{m})^2+(69\ \mu\text{m}/p_t)$$

for tracks with momentum p_t, measured in units of GeV/c. A rough estimate gives a resolution for the impact parameter $\sigma_b(\mu^+\mu^-)=21$ μm. In Fig. 14 we show a photograph of the display containing a candidate for the event $Z^0\to b\bar{b}$.

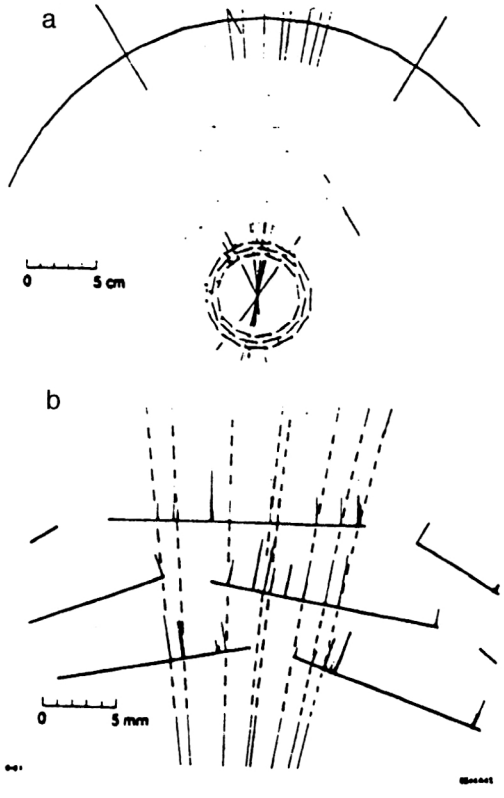

FIG. 12. (a) A reconstructed Z^0 decay from the Mark II microvertex detector; (b) a blowup of part of the picture.

Let us briefly consider the parameters of the microstrip detector. The detector width varies from 19.2 mm (384 microstrips) to 32 mm (640 microstrips) for the outer layer. The middle layer has 512 microstrips at a width of 25.6 mm. A semiconductor detector with integrated capacitative coupling and biasing resistors is used. In Fig. 15a we show the general form of a module of the microstrip detector. The electronic amplification and readout system is shown in Fig. 15b. The board on which the MX3 chips are mounted simultaneously forms a part of the mechanical construction of the microvertex detector. After the arrival of a common trigger signal, the pulses from the detector outputs are sequentially read out using a system of FASTBUS modules, then digitized and processed using a DSP56001 signal processor.

In Table III we give the parameters of four types of the best known microvertex detector used at the LEP and SLC accelerators.

The information readout is organized so that the data are read out every 50 μm (three microstrips per amplifier), and the values of the coordinates are calculated by the charge-division method. An MX3 readout chip is used; its parameters are given in Table IV.

More details about the characteristics of a number of VLSI chips designed for microstrip detectors can be found in Ref. 20.

The ALEPH microvertex detector. This is the first microvertex detector with double-sided readout, and it has been used in collider experiments since 1991. The general form of the detector is shown in Fig. 16. For this detector,[23] a special technology was used to construct a microstrip detector with double-sided readout, which allows two coordinates x and z to be recorded using a single detector surface.[24] The ALEPH detector consists of two concentric surfaces with

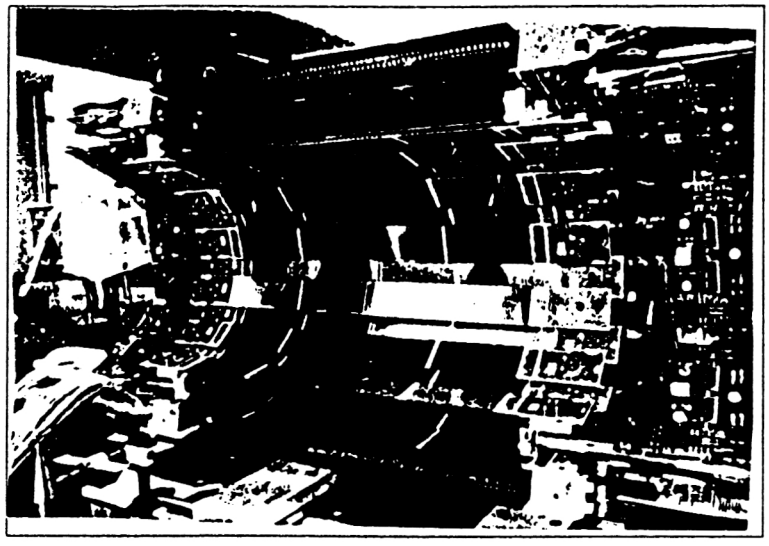

FIG. 13. General view of half of the DELPHI microvertex detector.

radii of 6.3 and 10.7 cm, covered with silicon microstrip detectors of area 0.25 m^2 ceramic holders, and an electronic readout system containing 74 000 recording channels. The microstrip detector with double-sided readout ideally solves the problem of recording the second (z) coordinate. This solution allows the signal magnitude to be optimized for minimum thickness of the material, and makes it possible to find the correlation of the amplitudes of pulses obtained from the charge collected on the two sides of the microstrip detector. The use of double-sided readout naturally leads to a significant improvement of the vertex detector and decreases the effect of particle multiple scattering. Therefore, the vertex detector for this setup contains only two concentric surfaces covered by microstrip detector modules. In Fig. 17 we give a schematic diagram of the structure of the backing of a

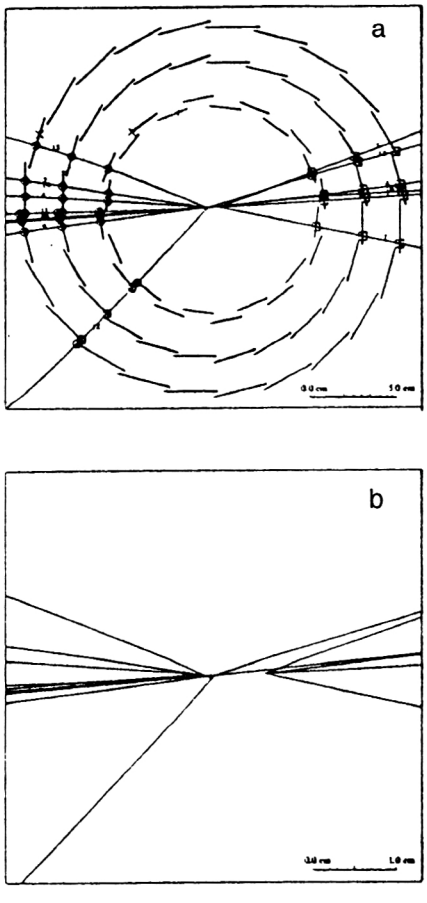

FIG. 14. Photograph of the display of a candidate for a $Z^0 \to b\bar{b}$ event recorded using the DELPHI microvertex detector.

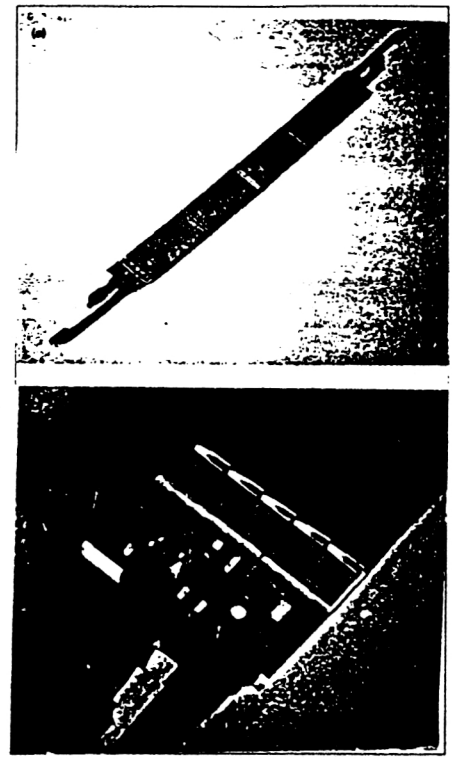

FIG. 15. (a) General view of an outer-layer detector module; (b) a data readout module.

TABLE IV. Parameters of VLSI chips used in semiconductor vertex detectors (Ref. 20).

Experiment	Mark II	DELPHI	ALEPH	OPAL	L3
VLSI chip	Microplex	MX3	CAMEX64A	MX5	SVX-H3
Type	5 μm NMOS	3 μm CMOS	3.5 μm CMOS	1.5 μm CMOS	3 μm CMOS
Number of channels	128	128	64	128	128
Surface area, mm^2	6.3×54	6.5×6.8	6.4×5.0	6.5×6.8	6.3×6.8
Strip, μm	47.5 (4 rows)	50 (2 rows)	100	550 (2 rows)	48 (2 rows)
Power dissipation, mW	14	0.75	1	2	1.3
Equivalent noise charge, e^-	$280+97C_{in}$	$350(C_{in}+3.5)^{1/2}$	$335+35C_{in}$	$325+23C_{in}$	$350+58C_{in}$
Radiation tolerance, krad	20	15	12	5	20

microstrip detector. It has dimensions 5.12×5.12 cm^2 and thickness 300 μm. The backing is made of high-resistance silicon, with p^+ microstrips implanted on the ϕ side with a pitch of 25 μm. Perpendicularly oriented n^+ microstrips are implanted on the opposite z side with a pitch of 50 μm. The signal on the ϕ side is read out from every fourth microstrip, and that on the z side is read out from every second one, so that the readout spacing on each side is 100 μm. The microvertex detector consists of 28 modules arranged in two layers. In turn, each module consists of two microstrip detectors with double-sided signal readout. On the p^+ side the strips of the two detectors are connected in series. The length of the strips on this side is 46.1 mm, and each detector has 483 channels. The total number of readout channels from a single base module is 1442, and the total number of recording channels is 81 000. The VLSI CAMEX64 chip used for data reading and recording has 64 independent channels, each of which contains a charge-sensitive preamplifier with controllable feedback. The second amplifier together with switched capacitors ensures double correlation sampling and additional gain. In 1991 the ALEPH vertex detector was used to record about 300 000 hadronic Z^0 decays. In Fig. 18 we show typical hadronic events from Z^0 decay in the $r-\phi$ and $r-z$ projections. The particle coordinates are determined by the charge-division method.

The OPAL microvertex detector. There are two modifications of the OPAL microvertex detector. The first uses microstrip detectors with one-coordinate readout. In the second, it was possible, owing to special technology, to design a

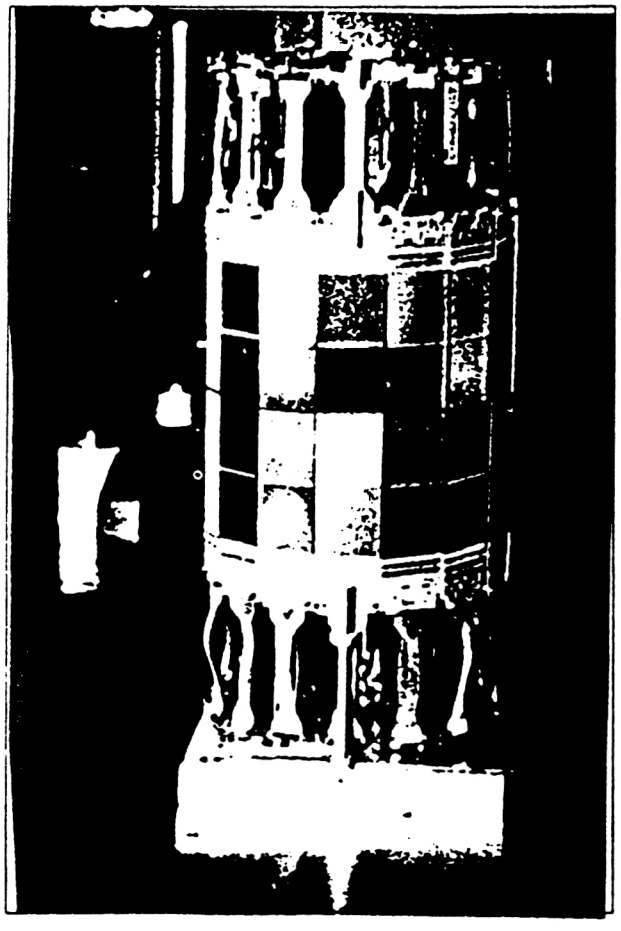

FIG. 16. General view of the ALEPH microvertex detector mounted on a graphite holding frame. Flexible printed leads are visible near the ends.

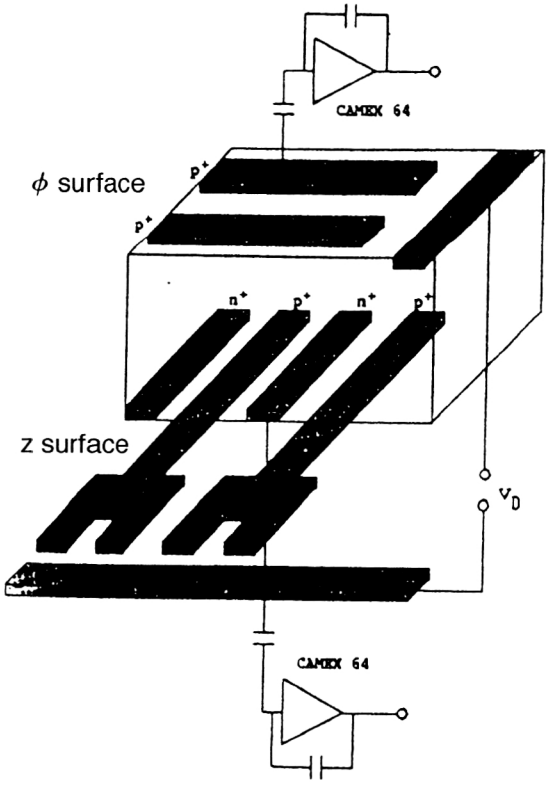

FIG. 17. Structure of the backing of the ALEPH microstrip detector with double-sided readout.

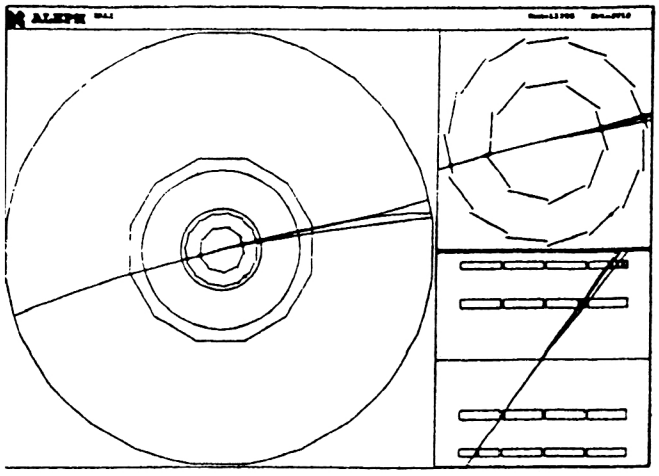

FIG. 18. Decay of a Z^0 boson into a pair of τ leptons containing one-prong and three-prong modes. On the left is a distorted view of the microvertex chamber, the inner tracking chamber, and the time-projection chamber. On the upper right is a more detailed picture of the tracks passing through the microvertex detector in the xy plane. On the lower right is the same event in the rz plane.

two-coordinate detector. The first version of the high-precision microvertex detector[27] was developed while the beam pipe at the LEP accelerator was being reconstructed, which led to the radius of the latter being decreased from 8.5 to 5.5 cm in 1991. The basic parameters of the microvertex detector are given in Table III. The detector consists of two concentric surfaces with radii 6.2 and 7.7 cm. The microstrips are oriented in the azimuthal (ϕ) direction with a pitch of 50 μm. For this reason it is possible to record only a single coordinate of a triggering particle. A special feature of the microstrip detector is the use of a field-effect transistor as the bias source for the individual implanted microstrips (the FOXFET structure),[28] which allows the dynamic resistance to be varied from 10 to 40 MΩ and improves the signal-to-noise ratio to 22:1. A microstrip module of the detector consists of three semiconductor detectors of length 6 cm connected as a sequential chain. Each such detector consists of 629 microstrips. The microstrip outputs are connected to amplifier inputs via a variable current. The total number of analog-signal readout channels is 16 000. The signals are recorded using a 128-channel MX5 VLSI chip (see Table IV), constructed using 1.5 μm CMOS technology. Each channel of the microcircuit has a charge-sensitive amplifier at the input. The output of the amplifier is connected to a storage capacitor. The signals from the capacitors of all the channels are read out using a 128-bit shift register. In 1991 the vertex detector was used to record about 250 000 hadronic Z^0 decays. A high resolution of order 15 μm was obtained for the impact parameter.

The modified version of the OPAL microvertex detector with two-coordinate readout is described in Ref. 28. The readout scheme that is used is fundamentally different from that of the ALEPH detector. This is in part due to technical difficulties. Readout of the second z coordinate is accomplished by simply gluing together the two surfaces of microstrip detectors oriented in the ϕ and z directions. Gold contacts laid down on a glass substrate are used to transfer signals corresponding to the z coordinate to amplifiers located in the same region as the readout amplifiers for the ϕ coordinates. In Table V we give the parameters of a microstrip module.

TABLE V. Parameters of a microstrip module of the modified OPAL detector.

Parameter	ϕ side	z side
Silicon thickness, μm	250	250
Microstrip pitch, μm	25	25
Readout microstrip pitch, μm	50	100
Individual resolution, μm	5.0	13
Number of readout channels	629	584
Signal-to-noise ratio (at peak)	24	20

Instead of an MX5 VLSI chip, the modified version of the detector uses an MX7 chip. This leads to a significant increase of the radiation tolerance and raises the noise stability by 20%. Individual coordinate resolutions of 5 μm and 13 μm in the ϕ and z coordinates, respectively, are obtained. The general parameters of the OPAL microvertex detector are given in Table VI.

A photograph of the OPAL microvertex detector built around the beam pipe at the LEP accelerator is shown in Fig. 19.

The L3 microvertex detector. The L3 microvertex detector[29–31] was introduced into experimental work fairly recently (at the beginning of 1993). Altogether, the detector consists of two concentric layers of cylindrical shape with radii 6.1 and 7.8 cm. Each layer contains 12 microstrip modules of thickness 300 μm and area 7×4 cm^2. Each in turn consists of two microstrip detectors with double-sided readout, so that the two particle coordinates z and $r-\phi$ can be measured. The expected single-track resolution is 7 μm and 14 μm in the $r\phi$ and rz planes, respectively. A special feature of the L3 microvertex detector is the fact that the outer layer of modules is shifted relative to the z axis by a stereoangle of 3°, which allows the identification of multitrack events. The construction and characteristics of the modules are described in more detail in Ref. 29. The microvertex detector ensures the reconstruction of particle tracks in polar angles of 22° and 158° and in an azimuthal angle of 360°.

TABLE VI. Parameters of the OPAL microvertex detector.

Parameter	Value
Number of layers	2
Number of microstrip detectors:	
inner layer	11
outer layer	14
Effective radius of a layer (mm):	
inner	61
outer	75
ϕ acceptance:	
inner layer	88%
outer layer	91%
Number of channels	30325
Cooling system	Water

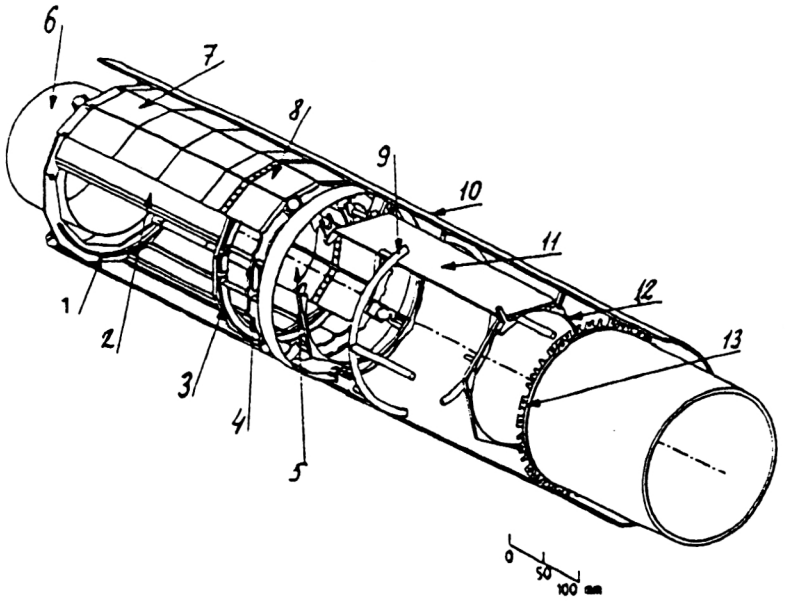

FIG. 19. General view of the OPAL detector. (*1*) Supporting ring; (*2*) beryllium shell; (*3*) supporting and cooling ring; (*4*) supporting ring; (*5*) inner detector plates; (*6*) beryllium beam pipe; (*7*) outer detector plates; (*8*) microcircuits; (*9*) cooling system; (*10*) pressure pipe; (*11*) plates for recording electronics; (*12*) supporting ring; (*13*) guides for cables.

The 128-channel SVX VLSI chip used for data readout contains all the circuitry required for data amplification, storage, and multiplexing for a single output channel, which is connected to the input of an optical transmitter. A functional board with optical decoupling also contains an 8-bit parallel ADC, which is used to digitize signals arriving from the detector, and 8-bit DACs used to set the ADC threshold and calibrate the SVX module. The outputs of the functional boards with optical decoupling are connected to the inputs of the data collection and processing system in the VME standard based on a TSM 99105 microprocessor.

The CDF microvertex detector. The CDF microvertex detector[32–34] is designed to perform experiments at the Fermilab pp collider and began operation in 1992. The problem was to ensure a track recording accuracy of order 10 μm. A general view of this detector is given in Fig. 20. It has four concentric layers. The inner and outer layers have radii 3.005 and 7.866 cm, respectively. The detector is located inside a vertex time-projection chamber. In Table VII we give the parameters of this microvertex detector.

The CDF detector consists of four layers of microstrip detectors with one-sided readout (on the order of 40 000 channels). The microstrip size is 25 μm, the spacing between the microstrips is 60 μm in the inner layer and 110 μm in the outer layer, the length is 8.5 cm, and the thickness is 300 μm. The microstrip detector modules have a maximum length of 510 mm, and each consists of three microstrip detectors. The characteristics of the 128-channel chip used for signal amplification and detection are given in Ref. 32. Each event produces 60–100 kilobytes of data.

The microvertex semiconductor detectors for the ATLAS experiment. A complex system of track detectors including several types of semiconductor microvertex detector is being planned for the future ATLAS experiment.[35] The tracking system is shown in Fig. 21. Two designs are being considered at present. In this section we shall briefly describe the microvertex semiconductor detectors. The main requirements on the inner microvertex detector are the following: (1) high spatial resolution of order 5–10 μm; (2) fast operation: the total charge collection time should be 20–30 nsec for detectors of thickness 300 μm; (3) high two-track resolution, a typical value being 150 μm; (4) high radiation stability. The inner microvertex detector consists of three concentric planes, located between 10 and 30 cm from the beam pipe. It is assumed that microstrip detectors with double-sided readout or two-coordinate (pixel) detectors will be used. These will allow the impact parameter to be measured with an accuracy of 25 μm.

A microstrip detector based on GaAs will allow the momentum resolution to be improved in a region with a high level of radiation. The third outer semiconductor detector in combination with the inner detector will ensure the accurate

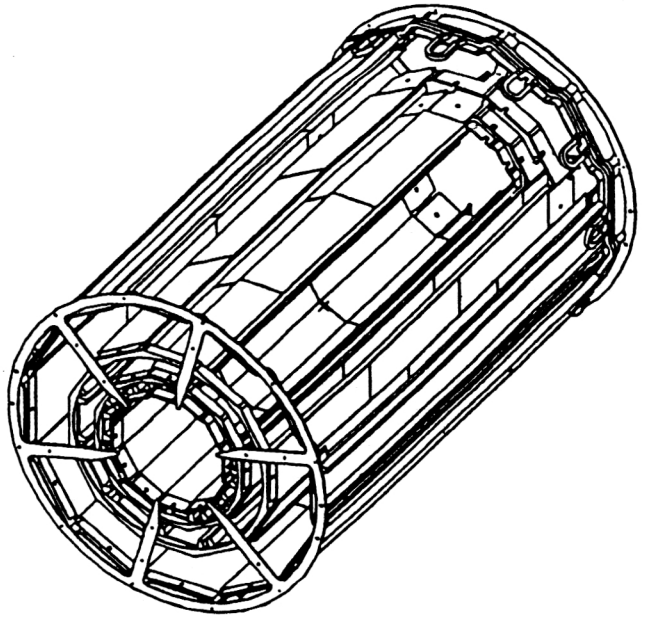

FIG. 20. General view of the CDF detector.

TABLE VII. Parameters of the CDF microvertex detector.

Parameter	Value
Number of layers	4
Inner/outer radius	3.005 cm/7.866 cm
Microstrips:	60 μm for layers 0–2, 55 μm for layer 3
Active length	51 cm (2×25.5)
Resolution	10 μm (impact parameter)
Technology	one-sided readout
Signal-to-noise ratio	9–10
Number of channels	46080
Number of chips	360
Power dissipation	175 mW/chip
Total power dissipation	100 W
Readout time	1–2 msec
Cooling	water, 14°
Beam intersection period	3.5 μsec

measurement of charged-particle pulses in the central region of the tracking system and data output for a second-level trigger.

The microvertex semiconductor detector for the CMS experiment. The structure of the cylindrical part of the CMS detector,[36] which consists mainly of microstrip gas detectors, will be discussed below. The main requirements on the microvertex detector are that it ensure a spatial resolution of 25 μm in the $r-\phi$ coordinates and a high momentum resolution. Detailed studies have shown that microstrips of length 125 mm and pitch 50 μm ensure the qualitative track reconstruction and satisfactory momentum resolution. The detector capacitance, which is important as it affects the noise level, must be less than 10–20 pF.

Requirements on the electronics of microvertex detectors. A silicon detector does not possess internal amplification, so that the charge arriving at the amplifier input is equal to the number of electron–hole pairs created in the passage of a charged particle. A signal equivalent to 25×10^3 electrons can be obtained from a standard crystal of thickness 300 μm. Therefore, silicon detectors require high-quality, low-noise amplifiers. It has been shown in Ref. 37 that of the three types of preamplifier (charge-sensitive, current, and voltage), the voltage type is best suited for experiments in high-energy physics. Owing to the stability of the output capacitance of the detector, it is possible to integrate the output signal directly at the amplifier input. In addition, a voltage amplifier has better noise stability than a charge-sensitive one. The amplifiers for microstrip detectors are usually realized in hybrid technology. The authors of the study cited above also considered methods of signal shaping and gating needed for noise filtering and digitization using ADCs.

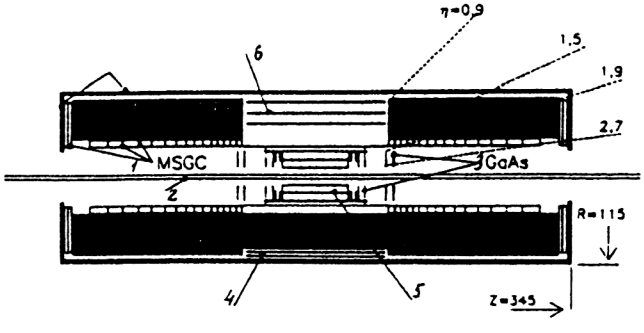

FIG. 21. Cross section of the system of track detectors of the ATLAS setup. (*1*) Microstrip gas counters; (*2*) ion duct; (*3*) GaAs semiconductor detectors; (*4,5*) semiconductor detectors.

The large number of recording channels in vertex detectors makes it necessary to devise an economical scheme for data readout from the detector planes. The problem is that it is difficult to make the small size of the detector crystal compatible with the actual size of the recording electronics. Therefore, the latter are realized as separate chips. An efficient monolithic chip is described in Ref. 38. It was realized by CMOS technology and contains 128 recording channels. The noise stability in the preamplifier circuit is increased by double-correlated sampling. A module has one output from the shift register. It is important that the required power per channel not exceed 1.6 mW. A two-module 64-channel system with buffer memory of the FIFO type is described in Ref. 39. It allows the data-readout rate to be increased significantly. The first module contains amplifiers and comparators, and the second is designated for data storage. The memory operates in the first-in–first-out mode, which allows only useful events to be recorded as trigger signals arrive.

A very promising direction in electronic readout systems for microstrip detectors is the use of capacitors which can be switched by means of transistor switches operating in conveyer mode. A signal is transferred (shifted) from one capacitor to another very quickly in such a memory. The problem is that for future collider experiments, where the number of readout channels in microvertex detectors can reach 10^5 and more, it is necessary to design noise-stable chips with low power requirements. In addition, an important defect of the chips which are used at present (their parameters are given in Table IV) is that they are not suitable for operation in the conveyer mode typical of collider experiments with small particle-bunch intersection period. It is well known that this time (16–96 nsec) is very small compared to that for the operation of a first-level trigger system (of the order of 1–2 μsec). The authors of Ref. 40 describe an analog delay and buffer realized using 1.2 μm CMOS technology and designed to record data from semiconductor detectors. After amplification by a charge-sensitive amplifier, the signals are sent to the input of a CR-RC shaper with a peaking time of 45 nsec. Then the shaped signals are moved to the analog buffer, which produces a delay of 1.2 μsec. After the arrival of the first-level trigger signal the analog samples are sent to the next level of the conveyer, where signals are processed with a frequency of 100 kHz.

Since analog memory devices are also used in pixel detectors (see below), let us briefly consider their operating principles.[41] In Fig. 22 we show a block diagram of a single channel of analog memory on switched capacitors. The analog signal is sent to the memory input via a low-ohm switch S1. A memory cell consists of a complementary switch (of n- and p-channel transistors, the drains of which are connected in parallel) and a double polysilicon capacitor of ca-

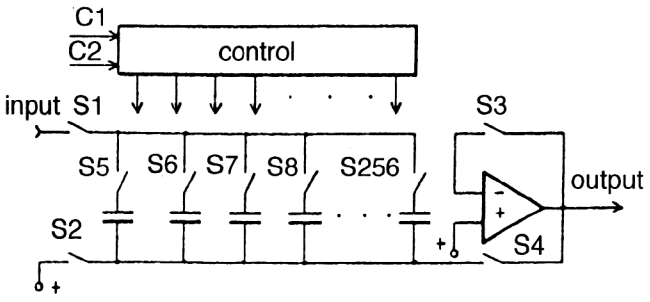

FIG. 22. Switched-capacitor analog memory channel. S1–S256 are switches, and C1 and C2 are clock pulses.

pacitance 1.5 pF with dielectric thickness equal to 700 Å. The input signals are shifted at the instant the clock pulse arrives at the two transistors (the depiction of the switches in Fig. 22 is simplified). An external reference voltage is applied to the bottom plates of the capacitors by means of the switch S2. As a result, the voltage stored in each capacitor at the time of the shift corresponds to the difference between the voltage of the input signal and the reference voltage. The switches S1 and S2 are closed before reading. The input signal bus and the bottom plates of the capacitors are thereby disconnected from the memory input and connected to the amplifier output by the switch S4. The signal recording frequency can reach 100 MHz. The concept of switched capacitors is also used effectively in the design of a 32-channel analog memory.[42]

4. MICROSTRIP GAS DETECTORS

Microstrip gas detectors were first described in Refs. 43 and 44. The prototypes of such detectors are multiwire proportional chambers and microstrip semiconductor detectors. In Fig. 23 we show the design of the detector described in Ref. 45. It consists of an insulating backing, on which are formed thin metallic anode and cathode strips several microns thick. The typical dimensions of the anode and cathode microstrips are 10 and 80 μm, and their pitch is 100 μm. The potential difference between the anode and cathode electrodes produces an electric field near the anode microstrips which is strong enough to ensure gas amplification of the electrons. The cathode electrodes are located at a distance of several millimeters above the surface in order to guarantee electron drift in the direction of the anode microstrips and to ensure the formation of a detectable signal. Just as in an ordinary multiwire proportional chamber, there is, in addition to the negative signal formed near the electron cloud, an induced pulse of positive sign at the neighboring cathodes, which allows improvement of the spatial resolution of the detector and makes it possible to record a second particle coordinate.

The technique of microstrip gas detectors is considered promising for future collider experiments. The new detectors have the following positive features: relative simplicity of construction, low cost, and high radiation tolerance. Another very important feature is that the gas amplification allows simplification of the readout electronics. Finally, the speed at which these detectors operate is higher than that of multiwire

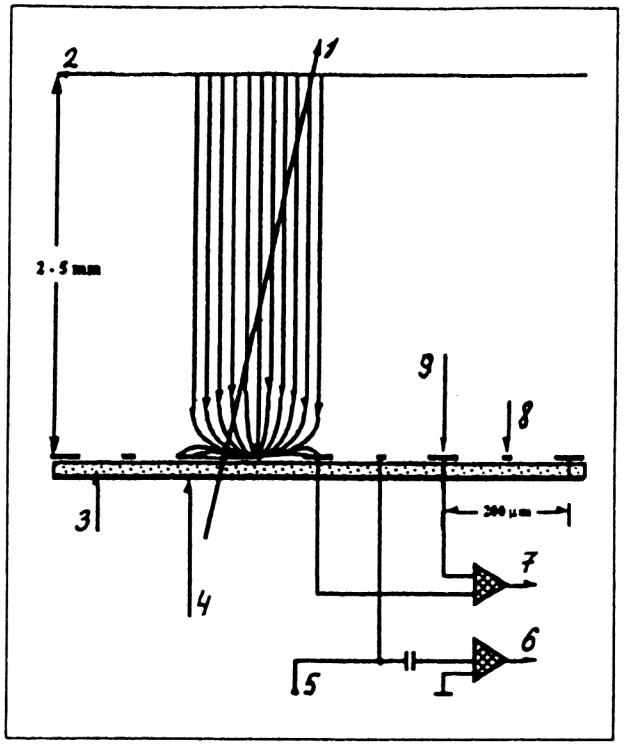

FIG. 23. Diagram of a microstrip gas detector. (*1*) Charged-particle track; (*2*) cathode surface; (*3*) backing; (*4*) electrode; (*5*) high voltage; (*6*) digital output; (*7*) analog output; (*8*) anode surfaces; (*9*) field strips. The thickness of the backing is 150–500 μm.

proportional chambers. In Fig. 24 we show a curve characterizing the relative gain as a function of the readout rate. For comparison, in Fig. 25 we give the values of this parameter for the microstrip gas detector.[46] We see that the microstrip gas detector can operate at fluxes exceeding 10^6 particles/mm^2·sec.

Recently, a large number of studies have been carried out to see how microstrip gas detectors can be improved. For example, Ref. 45 is devoted to studying the effect of various mixtures of gases on the detector characteristics. It has been shown that two gas mixtures, Xe/DME/CO_2 in proportions 30/30/40 and DME/CO_2 in proportions 60/40 (DME is dimethyl ether), are very promising for obtaining high resolution. Good efficiency and a resolution of 30 μm have been obtained in a gas volume of thickness 2.8 mm. The authors of Rev. 47 describe the design and construction of a microstrip gas detector distinguished by large surface area (10×10 cm^2) and allowing signal readout from both the anode microstrips and the cathode pads. The advances in this detector technique are generalized in Ref. 48. The accuracy of determining the coordinate for a minimally ionizing particle is 30 μm, which is better than the accuracy of drift chambers and approaches that of semiconductor microstrip detectors. The readout rate is high (above 10^6 mm^{-2} sec^{-1}), and the energy resolution is good. The authors of Ref. 49 present the results of using microstrip gas detectors in the Na12 experiment. Eight surfaces with a total of 1100 readout channels were used. The project for using microstrip gas surfaces inside a compact muon solenoid (CMS) as the

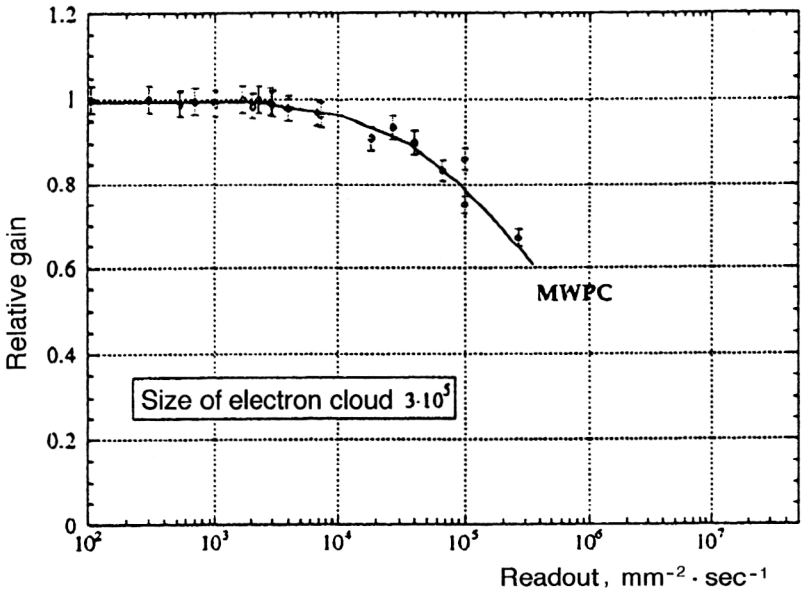

FIG. 24. Loading characteristic of the multiwire proportional chamber.

central detector is described in Ref. 50. The tracking system has two components: a forward section and a multilayer detector of cylindrical shape. The cross section of this detector in the rz plane is shown in Fig. 26. The central layer of the setup is a semiconductor microstrip detector, with the detector elements arranged parallel to the beam axis. The second and third layers consist of microstrip gas detectors having linear dimensions of 100×100 mm^2 and thickness 2–3 mm. In turn, each layer is divided into individual superlayers, as shown in Fig. 27. The accuracy of recording coordinates for discrete readout should be 40 μm, and for readout from the cathode pads it should be at least 30 μm. In the forward part of the CMS microstrip gas detector the detector elements are arranged radially relative to the beam axis. The use of a detector with a high degree of discreteness over the entire volume improves the accuracy with which charged-particle momenta and coordinates are measured, and simplifies the construction of the detector as a whole.

Two-coordinate microvertex detectors.. A pixel (two-coordinate) detector is a semiconductor device with a large number of detector elements arranged on a plane. Pixel microvertex detectors have several advantages over one-coordinate detectors. For example, the determination of the coordinates of n particles using a one-coordinate detector plane generates n uncertainties ("ghosts"). If a microstrip detector has two surfaces, then n^2 ghosts are obtained in the track reconstruction. The unique reconstruction of multitrack events requires a detector consisting of six planes.[51] This approach is not feasible, owing to such factors as the thickness of the material, the power dissipation, the readout time,

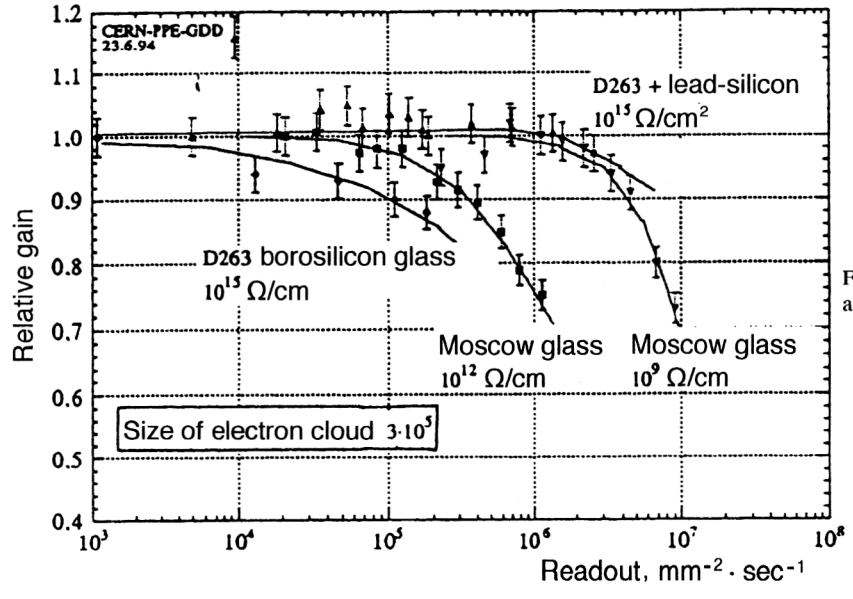

FIG. 25. Rate characteristics of the multistrip gas detector as a function of the conductivity of the backing.

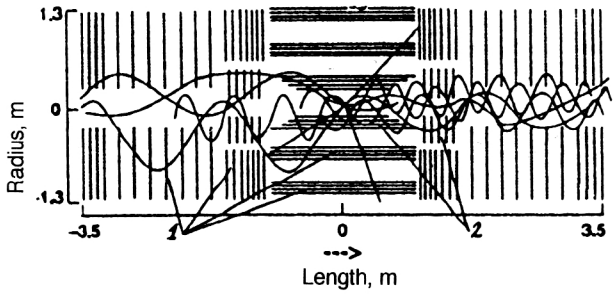

FIG. 26. View of the solenoidal detector CMS in the $r\phi$ plane. (*1*) Microstrip gas counters; (2) silicon detectors.

and so on. Therefore, pixel detectors are more promising. CCD matrices and silicon detectors are the most widely used types.

Pixel detectors based on CCD matrices. Pioneering studies of charge-coupled devices (CCDs; Ref. 52) have shown that CCD matrices can be used successfully in the design of precision elementary-particle detectors, including vertex detectors. The typical CCD matrices used as detectors have the following characteristics: a spatial accuracy of 3 μm, a two-track resolution of 60 μm, a time resolution of 500 nsec, a readout time of 4–5 msec, and a radiation tolerance of 3×10^5 rad, which is equivalent to one year of operation in a beam with 10^6 particles per bunch. Like microstrip detectors, CCD matrices are used in both fixed-target and collider experiments. The principles of operation of CCD matrices are described in detail in Ref. 53. The active area of the matrix is usually 1 cm^2 and the dimensions of a single cell are 22×22 μm. In the NA32 experiment, the vertex detector contains eight microstrip detectors in addition to the CCD matrices. Since the CCD matrices can operate when the track density is high, they are placed closer to the target. The accuracy of recording the primary interaction vertex in this detector is 2 μm (Ref. 54).

In fixed-target experiments a telescope of CCD matrices is used in combination with an active target. A minimally ionizing particle generates a charge in the detector equal to 1000 electrons, and to decrease the noise level the detector is placed in a cryostat at liquid-nitrogen temperature. Two

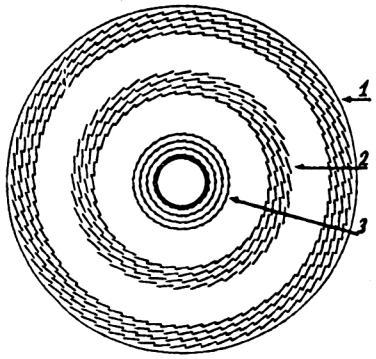

FIG. 27. View of the solenoidal detector CMS in the $r\phi$ plane. (*1*) Outer microstrip gas counters (chambers), with 68 counters per layer; (*2*) inner microstrip gas counters, with 40 counters per layer; (*3*) semiconductor microstrip detectors.

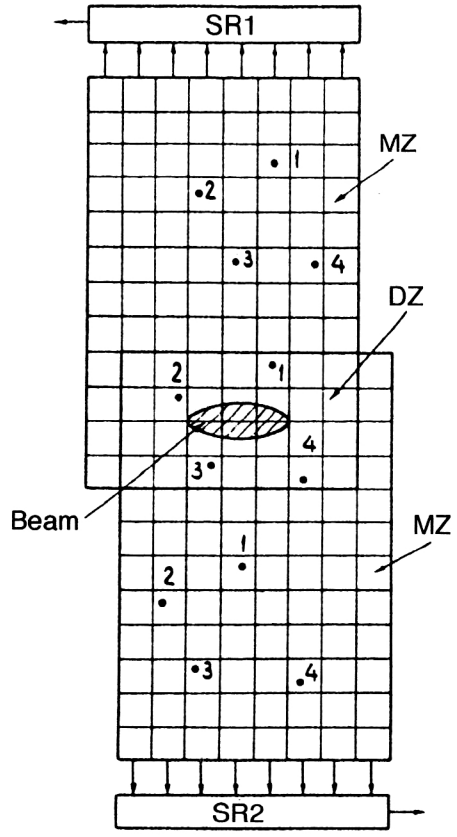

FIG. 28. Method of combined data collection and storage used in CCD-based microvertex detectors. SR1 and SR2 are shift registers. MZ is the memory zone, DZ is the detector zone, and 1–4 are used cells.

methods have been developed for data readout from CCD matrices used as detectors. In the first,[55] two CCD matrices are arranged so that they only partially overlap (Fig. 28). Two zones are obtained as a result. The common zone is used as the detector, and the rest is used as memory. The readout is done at a rate of 1 MHz and in opposite directions, which simplifies the track identification. When a particle bunch arrives, the data are moved to memory, and after the arrival of a trigger signal the input of clock pulses ceases. Then the data is read into the external memory. In the other method, tracks unrelated to the trigger signal are distinguished.[56] The data from even and odd matrices are read out in opposite directions. In the track reconstruction process it is assumed that the signals arriving from the particle of interest have equal readout time (in units of the clock frequency). The authors of that study describe a CCD matrix with a clock frequency of 6.75 MHz which functions at room temperature and contains 2.3×10^5 cells (576 columns with 385 cells in each).

The SLD microvertex detector. This detector is designed for use in experiments performed at a linear collider.[51] At present there are two versions of the detector, referred to as SLD1 (Ref. 51) and SLD2 (Ref. 57). An overall view of the two halves of the SLD1 detector is given in Fig. 29. It consists of four concentric layers, covered on both sides with CCD matrices. The radii of the outer and inner layers are 41.5 and 29.5 mm. Altogether, there are 480 CCD matrices containing 120×10^6 pixels. The CCD matrices are mounted

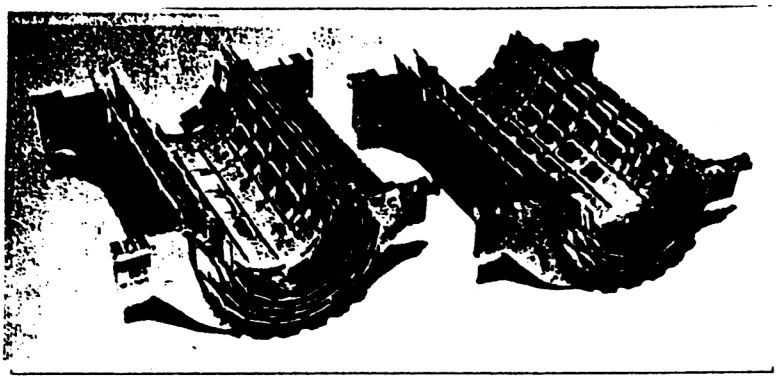

FIG. 29. General view of the two halves of the SLD microvertex detector.

on 60 modules with eight matrices on each module. The modules are mounted on two half-cylinders made of beryllium. The CCD matrices themselves are prepared on a silicon backing and have a pixel area of 20 μm^2. Altogether, there are 16×10^6 pixels on the backing. Since it is an order of magnitude thinner than a microstrip detector, a detector based on CCD matrices gives a better resolution for inclined tracks (of order 5 μm). In order to optimize the radiation losses and decrease noise, the detector is placed in a cryostat at a temperature of 180 K. Such detectors have the following advantages.[57] (1) The cells are highly discrete, and there is no high supply voltage or any means of charge multiplication. Therefore, the detector possesses high noise stability. (2) The near absence of clusters simplifies the track fitting. (3) Two coordinates are obtained at each point on a track. (4) Use over a period of three years has shown that the detector is highly stable over time. In Fig. 30 we show the impact-parameter distribution in the xy and rz planes for tracks from Z^0 decay. The following basic parameters were obtained: spatial resolutions of 5 μm and 6 μm in the xy plane and in the z direction, respectively. The impact parameter was measured for two tracks with large curvature, using a muon pair from Z^0 decay. A Gaussian fit gave the following for the single-track resolution: 11 μm for xy and 38 μm for rz.

The parameters of the SLD1 and SLD2 microvertex detectors are compared in Table VIII (Ref. 57).

The SLD2 microvertex detector should be introduced into experiments in 1995. We see from Table VIII that the detector was constructed using specially designed CCD matrices of large dimension and with increased time parameters, which allows a decrease of the readout time and improves the resolution in the impact parameter. Since the bunch collision frequency at the SLAC accelerator is only 120 Hz, the large time for signal readout from the detector, of order 160 msec, will not affect the efficiency of operation of the CCD matrices.

5. SILICON TWO-DIMENSIONAL RECORDERS

The question can be posed of how to design a two-dimensional recorder which simultaneously combines all the advantages of silicon microstrip detectors and CCD matrices and contains not only amplifiers, but also information transformers. The technical problems which arise are discussed in Ref. 58. Using modern technology, it is not difficult to fabricate 10^6 diodes arranged in the form of a matrix on a single crystal. The problem is to make a device which is large enough and contains fast recording electronics with small power dissipation. The prototype silicon sensor described in

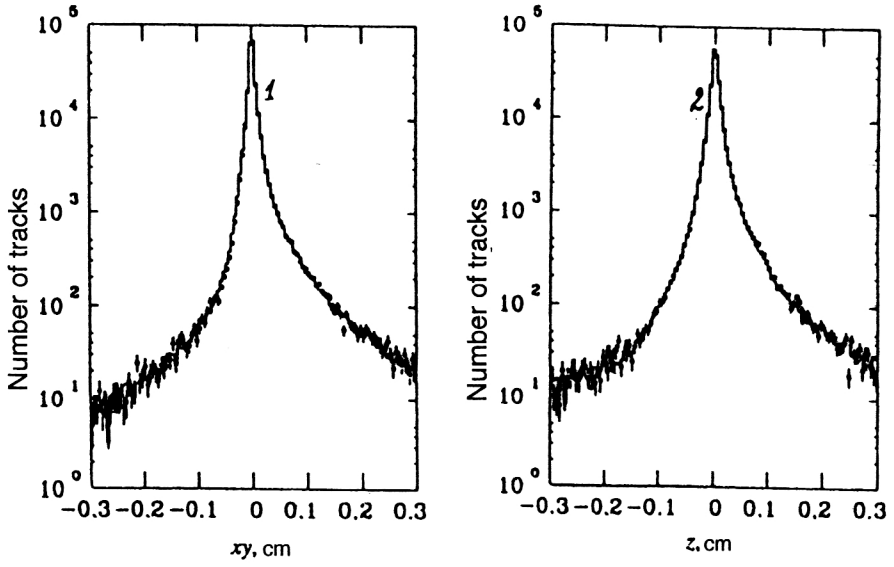

FIG. 30. Distribution of the impact parameter in the xy and rz planes for tracks belonging to hadronic Z^0 decay. (*1* Impact parameter in the xy plane; (2) impact parameter in the rz plane.

TABLE VIII. Comparison of the parameters of the SLD1 and SLD2 detectors.

Parameter	SLD1	SLD2
Number of layers	4	3
Number of modules	60	48
Number of CCD matrices	480	96
Number of pixels	110×10^6	307×10^6
Active dimensions of the CCD matrices, cm	1.3×0.9	8.0×1.6
Active length (z), cm	9.2	15.9
Number of pixels per track	2.3	3.2
Readout frequency, MHz	2	10
Readout time, msec	160	100
Impact parameter (xy), μm	$11+70/p$	$9+29/p$
Impact parameter (rz), μm	$39+70/p$	$14+29/p$

Note: The + sign denotes the sum of the squares; p is the momentum in GeV/c.

Ref. 59 has a detector containing 1024 diodes (32×32), a parallel ADC, and a coordinate encoder. The coordinate encoder is made from comparators, so that uncertainties arise in the encoding of multiple events. A more sophisticated device for sampling triggered columns and rows with subsequent encoding of the coordinates of the triggered cells is the priority encoder described in Ref. 60. In Ref. 61 the problem of designing a fast and economical signal readout system is solved by using a matrix of switched capacitors operating in the conveyer mode. Such a memory essentially is the microelectronic analog of an ordinary delay circuit. The memory operates in two phases: the sensitive phase, during which the detector is bombarded, and the data readout phase. In Fig. 31 we give the block diagram of a pixel detector with switched capacitor memory. The data are written into memory after exposure of the detector part of the module. The recording is done along columns, while the readout is done along rows at a rate of 100 MHz using a multiplexer. Then the data are sent to the common memory via an optical link.

Several semiconductor pixel detector modules with very good parameters have been developed recently. The authors of Ref. 62 describe a hybrid pixel detector containing a matrix of 96×378 (36 288) sensitive elements, located on an area of 75×500 μm^2. The module was designed for the WA97 experiment at CERN. In Fig. 32 we show a general view of six modules together with the processor board and the corresponding connectors. Each chip contains six matrices. A two-track resolution of at least 10 μm is obtained. Each sensitive element has its own signal amplification, discrimination, and recording channel. Figure 33 helps to illustrate the methodological possibilities offered by semiconductor pixel detectors in particle track reconstruction. The well known expression for finding the coordinates by calculating the center of mass of the signal is used to determine the particle coordinates accurately when clusters are present.[62,63]

6. VERTEX DETECTORS BASED ON SCINTILLATING OPTICAL-FIBER LIGHT GUIDES

The development of the technology of ordinary fiber-optics light guides, microelectronics, and optoelectronics has made it possible to design fast precision vertex detectors

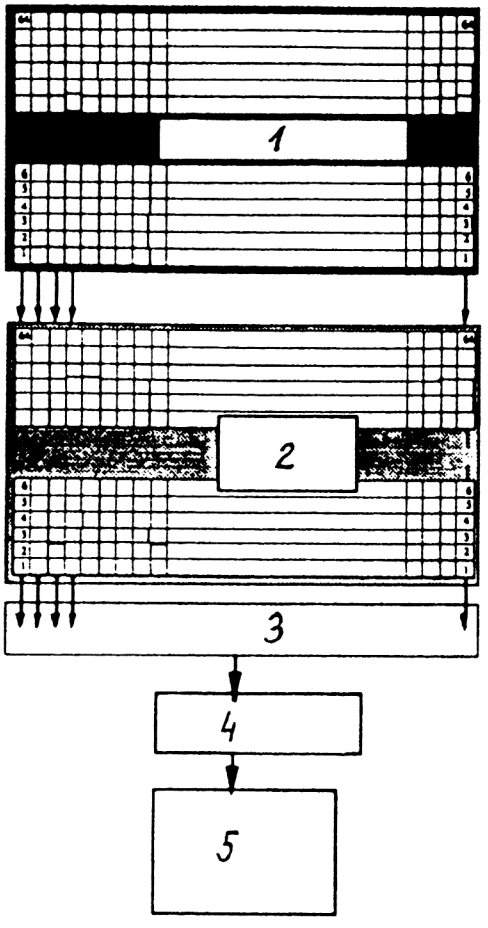

FIG. 31. Use of conveyer memory for signal readout from a two-coordinate detector. (*1*) Two-coordinate detector; (*2*) conveyer memory; (*3*) multiplexer; (*4*) optical link; (*5*) memory.

based on scintillating fiber-optics light guides (SCIFI detectors). Elementary-particle detectors using the beams of thin scintillators were first developed in the late 1950s.[64] However, their use did not become widespread, owing to the development of more efficient track detectors such as bubble and spark chambers. The reviews of Refs. 65 and 66 deal with the technical problems and various aspects of the use of scintillating optical-fiber light guides (SCIFIs) as elementary-particle detectors, active targets, track detectors, and also in the construction of calorimeters and so on. A SCIFI (Fig. 34) consists of a core made of plastic or glass scintillator covered by a material with small light transmission coefficient. In addition, there is an outermost thin covering of black glass. Plastic scintillators have the following advantages over glass ones: (1) the light yield is higher by a factor of 4 to 5; (2) the luminescence time is an order of magnitude smaller (3 nsec and 55 nsec, respectively); (3) the radiation tolerance is higher; (4) they are easier to manufacture. However, the glass-based SCIFIs used in experiments have an inner diameter of the order of 10 μm, compared to 50–500 μm for plastic SCIFIs. Plastic SCIFIs of diameter 30 μm have been made.[67] The characteristics of the two types of SCIFI are described in more detail in Ref. 68. It has been

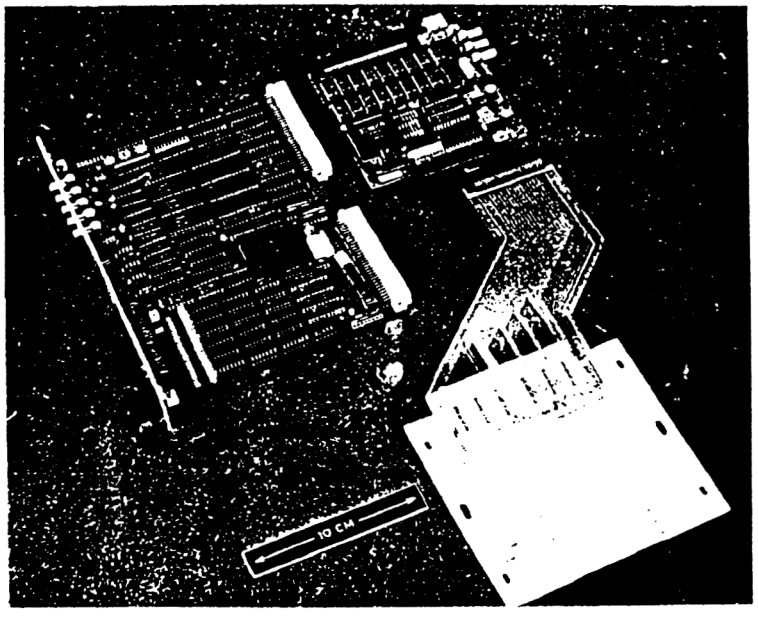

FIG. 32. Photograph of a matrix of six modules containing 32 288 detector elements together with processor boards.

shown that if a SCIFI of diameter 30 μm is used as the active target, it is possible to obtain a two-track resolution of order 20 μm.

The cross section of a SCIFI can be circular, rectangular, or even hexagonal. The two latter types of SCIFI can be used to construct detectors with a high density of scintillating material.[69] For the construction of an active target, individual SCIFIs are combined into bunches of cylindrical or square shape with a cross-sectional area of 15–20 mm^2 and a length of several centimeters. Depending on the physics of the events studied (the particle emission angle), the SCIFI bunch is oriented either perpendicular or parallel to the beam (Figs. 35b and 35c).[70] The light image of an event is essentially projected on the output light-sensitive surface of the first cascade of the optoelectronic system, where it is amplified and sent to the readout system. As an example, let us consider the use of SCIFIs in the construction of the precision vertex detector for the WA84 experiment at CERN.[71] The problem is to measure the lifetime of charged and neutral B mesons (Fig. 36). The B-meson decay length is $L=400$ μm. The complexity of the topology of the studied events and the short particle lifetime impose the following requirements on the vertex detector: (1) it must operate efficiently in an intense beam of at least 10^6 particles/sec; (2) it must have high radiation tolerance; (3) the track-recording accuracy must be 5 μm; (4) it must operate in the trigger mode; (5) it must allow measurement of the track curvature.

The vertex detector that we have described satisfies these conditions, because it is based on SCIFIs with a gatable optoelectronic data amplification and readout system incorporating a CCD matrix. In addition, the vertex detector includes

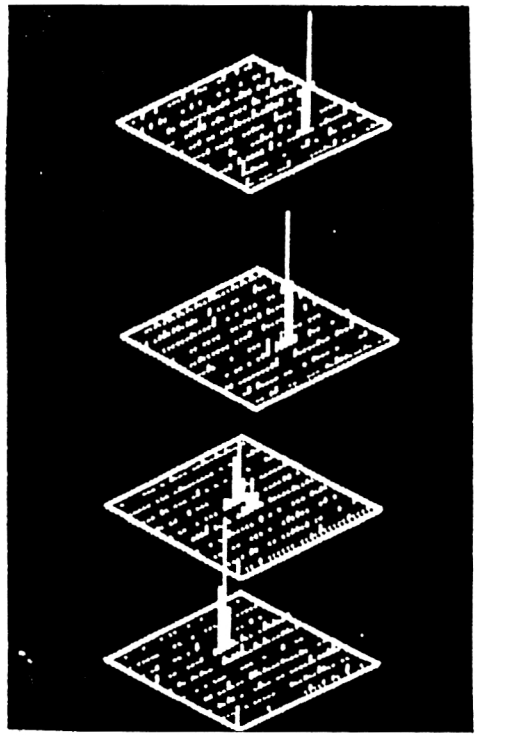

FIG. 33. Display of the passage of a charged particle through four planes of pixel detectors.

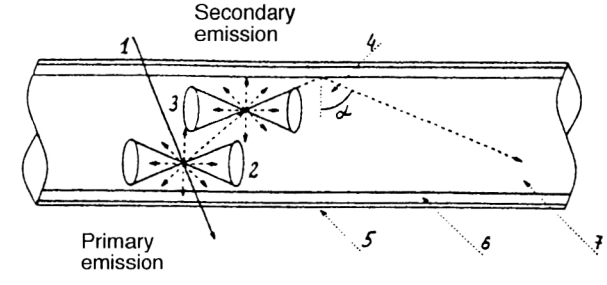

FIG. 34. Geometrical and optical parameters of a typical SCIFI. (*1*) Particle track; (*2*) primary emission; (*3*) secondary emission; (*4*) critical angle of reflection; (*5*) outer shell; (*6*) inner shell; (*7*); core.

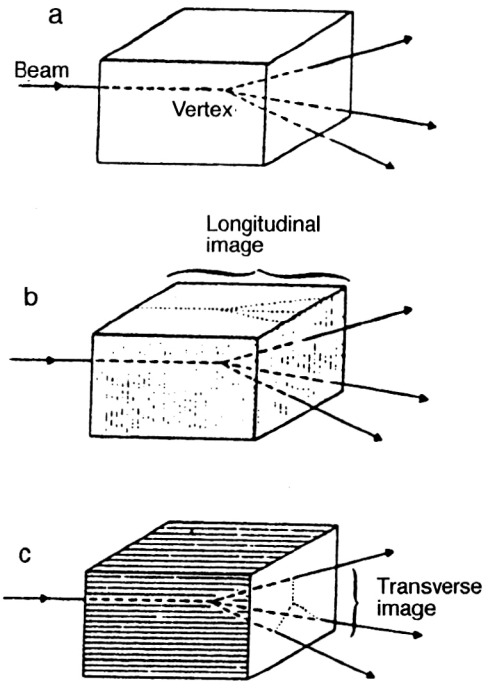

FIG. 35. Scintillation targets. (a) Solid scintillator; (b) and (c) SCIFI-based targets oriented perpendicular and parallel to the beam.

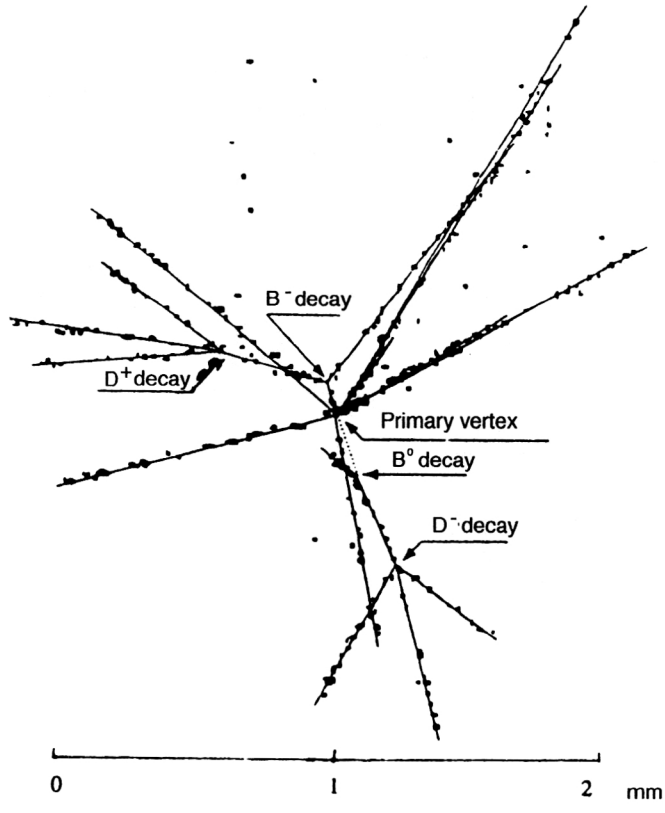

FIG. 36. General view of B^0 and B^- decay products in the plane perpendicular to the particle beam. Monte Carlo modeling was used. Four secondary vertices can be seen in addition to the primary decay vertex.

a telescope of microstrip semiconductor detectors, which allow more efficient reconstruction of the event topology. Owing to the weak light yield of an event in the target, an image intensification system is located between the target and the CCD matrix. This system is shown schematically in Fig. 37. Most image intensifiers cannot operate efficiently in a magnetic field, and so the active target is located in the forward part of the magnetic spectrometer. It consists of a parallel bunch of SCIFIs of diameter 30 μm arranged along the particle beam. The vertical component of the magnetic field is 1.8 T near the target, so that the five-cascade optoelectronic system is divided into two parts. The first part, which has a gain of 20, is located near the target. The light image of the event is sent to a region with a magnetic field of 0.1 T, using a light guide of length 2.5 m. The second part of the system, which is magnetically shielded, amplifies the event image by a factor of about 10^4 and sends it to the CCD matrix. As can be seen in Fig. 37, the target is optically connected directly to the fiber-optics light guide, which is followed by a pair of optoelectronic intensifiers with electrostatic focusing. The second part of the intensification system consists of three microchannel plates which operate in gated mode. The optoelectronic system is completed by a CCD matrix of volume 16×10^4 cells, which is divided into two zones: an image zone and a memory zone. The trigger system of the vertex detector has two levels. In the first, a scintillation telescope is used to shape a gate pulse for the optoelectronic system. This signal appears 80 nsec after the interaction. The second-level trigger signal arriving 400 nsec later is generated by scintillation hodoscopes and used as the start pulse for data readout from the CCD matrix. The sensitive area of the CCD matrix is 1 cm^2 so that it matches well the dimensions of the active target. There is also good matching between the individual SCIFIs and the cells of the CCD matrix (20×20 μm^2).

The SCIFI vertex detector was tested in an accelerator beam. The following results were obtained: (1) the average density of recorded points was 0.7 per mm; (2) the two-point resolution was 33 μm; (3) among the useful events there is a significant background arising from all the components of the vertex detector.[72]

The noise arising in SCIFI vertex detectors is analyzed in detail in Ref. 73 from both the theoretical point of view and by taking into account the experimental data. The main sources of noise are: (1) optical crosstalk in the target; (2) electron backscattering in the image intensifiers; (3) electronic noise in the CCD readout. In Fig. 38 we show an event recorded in a beam of 200-GeV particles, (a) without filtering and (b) processed using a program taking into account the value of the threshold and the pedestal in the CCD matrix.

The parameters of the optoelectronic system can be improved both by increasing the SCIFI light yield and by improving the quantum efficiency of the electro-optical transformers. The track detector described in Ref. 74 has a two-track resolution of 52 μm and measures the impact parameter with an accuracy of 9 μm. The event filtering and reconstruction are performed in the following sequence. 1. The most probable points of the track are reconstructed. For example, points associated with fewer than three bins are discarded. 2. Candidates for event tracks are drawn through

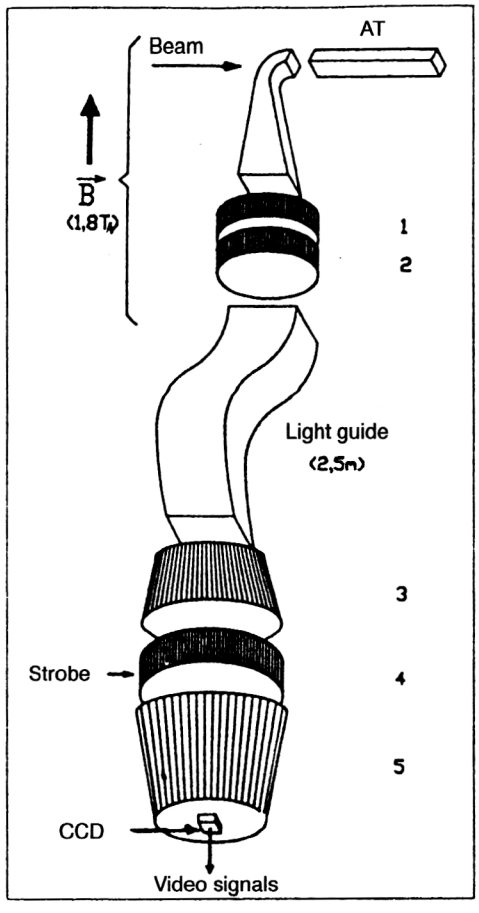

FIG. 37. Schematic view of the active target of the WA84 vertex detector. AM is the active target, and 1–5 are optoelectronic intensifiers.

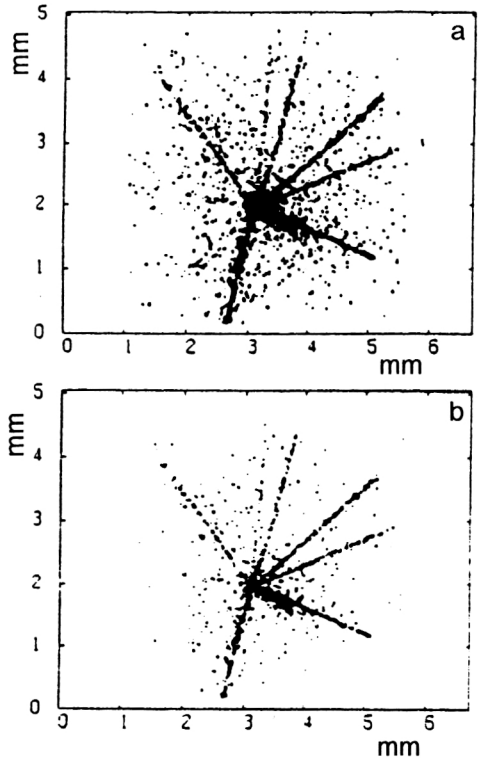

FIG. 38. Event topology (a) before and (b) after noise filtering.

the centers of the reconstructed points. 3. Given criteria are used to reconstruct useful tracks and event topologies.

If we compare SCIFI vertex detectors with semiconductor microstrip detectors, we find that, while they have about the same resolution, the former have only one readout surface, which considerably simplifies the data recording system. Perhaps their only weakness is the data readout time. However, owing to the rapid development and improvement of multianode and position-sensitive photomultipliers with operating rates of up to 100 MHz,[75–77] optoelectronic vertex detectors will be used more and more often, especially in collider experiments. A SCIFI vertex detector designed for such experiments has the form of a cylinder with four concentric detector planes. It is thought that the accuracy of measuring the impact parameter will be at least 20 microns.[78] The advantages of SCIFIs will stimulate further research with the goal of improving important parameters like the attenuation length λ, the distance at which the signal amplitude decreases by a factor of e. The authors of Ref. 79 describe the fabrication of a plastic SCIFI with $\lambda = 2.8$ m. This achievement significantly extends the range of SCIFI applicability in high-energy physics.

CONCLUSION

Semiconductor detectors accurately record event coordinates on the scale of microns and, owing to their highly developed technology, they can easily be mass produced and offer extensive possibilities when used as high-precision vertex detectors. However, silicon microstrip detectors with data readout from a single side of the crystal have the same defects as multiwire proportional chambers: it is difficult to reconstruct events with high multiplicity, and the use of such detectors in experiments requires a great deal of electronics and complicates the construction of the vertex detector. Therefore, the development of silicon microstrip detectors with double-sided readout will ensure the further development and use of detectors of this type in future experiments.

CCD matrices of the classical type differ in many respects from two-dimensional recorders with memory. In addition, the small size of a sensitive cell coincides well with the SCIFI dimensions. Therefore, CCD matrices are widely used to monitor light images in precision detectors based on SCIFIs. Perhaps the only drawback of the CCD matrices which are used is their low readout rate of tens of msec.

The development of silicon pixel detectors can be viewed as a new stage in the evolution of two-dimensional recorders. In pixel detectors, both the recording electronics and the data digitizing and encoding devices are located on a common substrate together with the sensitive cells.

Microvertex gas detectors, which have already begun to be used in experiments, offer broad possibilities for future experiments.

The development of SCIFI-based precision vertex detectors presents a new feature: the use of optical methods for detecting complex events. As a result, only one data-readout surface, a CCD matrix, is used in such a vertex detector. This leads to a sharp reduction in the number of readout channels.

In turn, the development of multianode photomultipliers containing up to 1024 discrete light-sensitive cells will make it possible in the future to increase the rate of operation of SCIFI-based vertex detectors.[80]

Microstrip gas detectors may also be used as vertex detectors in future experiments.

The rapid development of precision vertex-detector techniques stimulates the development of specialized integrated microcircuits and techniques for recording useful events and track reconstruction in real time. Along with the specialized processors developed directly for this type of detector, there is a trend to develop track processors of a universal type on the basis of fast programmable logic matrices.

[1] K. G. McKay, Phys. Rev. **84**, 829 (1951).
[2] G. Hall, Rep. Prog. Phys. **57**, 49 (1994).
[3] J. M. McKenzie, Nucl. Instrum. Methods **162**, 49 (1979).
[4] P. Rehak and E. Gatti, Nucl. Instrum. Methods A **289**, 410 (1990).
[5] V. Radeka, Nucl. Instrum. Methods **226**, 209 (1984).
[6] R. Klanner, Preprint MPI-PAE/Exp. E1.135, Max-Planck-Institute, Munich (1984).
[7] G. Batignani, F. Bosi, L. Bosisio *et al.*, Nucl. Instrum. Methods A **277**, 147 (1989).
[8] R. Barate, P. Bonamy, P. Borgeaud *et al.*, Nucl. Instrum. Methods A **235**, 235 (1985).
[9] S. R. Amendolia, G. Batignani, F. Bedeschi *et al.*, Nucl. Instrum. Methods A **226**, 78 (1984).
[10] M. Adinolfi, C. Angelini, D. Barney *et al.*, Nucl. Instrum. Methods A **329**, 117 (1993).
[11] G. Bellini, M. Giammarchi, P. F. Manfredi *et al.*, Nucl. Instrum. Methods A **252**, 366 (1986).
[12] J. F. Boland, W. Beusch, M. Dameri *et al.*, Nucl. Phys. (Proc. Suppl.) **1B**, 303 (1988).
[13] G. Darbo and L. Rossi, Nucl. Instrum. Methods A **289**, 584 (1990).
[14] G. Darbo and B. W. Heck, Nucl. Instrum. Methods A **257**, 567 (1987).
[15] G. Darbo and S. Vitale, Nucl. Instrum. Methods A **190**, 81 (1981).
[16] A. Beer, A. Corre, Ph. Farthouat *et al.*, Nucl. Instrum. Methods A **337**, 280 (1994).
[17] S. R. Amendolia, F. Bedeschi, G. Bellettini *et al.*, Nucl. Instrum. Methods A **289**, 539 (1990).
[18] B. Denby, Th. Lindblad, C. S. Lindsey *et al.*, Nucl. Instrum. Methods A **335**, 296 (1993).
[19] S. Gadomski and M. Turala, Nucl. Instrum. Methods A **344**, 125 (1994).
[20] A. S. Schwarz, Preprint MPI-PhE/92-05, Max-Planck-Institute, Munich (1992).
[21] C. Adolphsen, R. G. Jacobsen, V. Lüth *et al.*, Nucl. Instrum. Methods A **313**, 63 (1992).
[22] N. Bingefors, H. Borner, R. Boulter *et al.*, Nucl. Instrum. Methods A **328**, 447 (1993).
[23] P. Holl, H. Dietl, J. Fent *et al.*, Nucl. Instrum. Methods A **257**, 587 (1987).
[24] G. Batignani, C. Bauer, H. Becker *et al.*, Preprint INFN PI/AE 90/17, INFN, Pisa (1990).
[25] G. Batignani, C. Bauer, H. Becker *et al.*, Nucl. Instrum. Methods A **326**, 183 (1993).
[26] R. Brenner, R. Harr, A. Rudge *et al.*, Nucl. Instrum. Methods A **326**, 189 (1993).
[27] P. P. Allport, J. R. Batley, P. Capiluppi *et al.*, Nucl. Instrum. Methods A **324**, 34 (1993).
[28] P. P. Allport, J. R. Batley, G. A. Beck *et al.*, Preprint CERN-PPE/94-16, CERN, Geneva (1994).
[29] B. Alpat, G. Ambrosi, G. Barbagli *et al.*, Nucl. Instrum. Methods A **315**, 197 (1992).
[30] M. Acciarri, A. Adam, O. Adriani *et al.*, Nucl. Instrum. Methods A **351**, 300 (1994).
[31] G. Ambrosi, E. Babucci, R. Battiston *et al.*, Nucl. Instrum. Methods A **344**, 133 (1994).
[32] W. C. Carithers, R. P. Ely, C. Haber *et al.*, Nucl. Instrum. Methods A **289**, 388 (1990).
[33] B. Barnet, C. Boswell, J. Mathews *et al.*, Nucl. Instrum. Methods A **315**, 125 (1992).
[34] S. Tkaczuk, H. Carter, B. Flaugher *et al.*, Preprint CDF/PUB/SEC VTX/PUBLIC/2274, Fermilab-Conf-93/290-E, Fermilab, Batavia (1993).
[35] *ATLAS Letter of Intention*, CERN/LHCC/92-4, LHCC/12, CERN, Geneva (1992).
[36] *CMS, The Compact Muon Solenoid*, CERN/LHCC 92-3, LHCC/11, CERN, Geneva (1992).
[37] E. Gatti and P. F. Manfredi, Nucl. Instrum. Methods A **226**, 142 (1984).
[38] W. Buttler, G. Lutz, V. Bergmann *et al.*, Nucl. Instrum. Methods A **273**, 778 (1988).
[39] D. E. Dorfan, Nucl. Instrum. Methods A **279**, 186 (1989).
[40] R. Brenner, H. von der Lippe *et al.*, Nucl. Instrum. Methods A **339**, 564 (1994).
[41] S. A. Kleinfelder, IEEE Trans. Nucl. Sci. **NS-37**, 1230 (1990).
[42] D. Munday, A. Parker, F. Anghinolfi *et al.*, Nucl. Instrum. Methods A **326**, 100 (1993).
[43] A. Oed, Nucl. Instrum. Methods A **283**, 351 (1988).
[44] F. Angelini, R. Belazzini, A. Brez *et al.*, Nucl. Instrum. Methods A **283**, 755 (1989).
[45] F. Sauli, Preprint CERN-PPE/94-150, CERN, Geneva (1994).
[46] M. Geijsberts, F. G. Hartes, J. G. Pannekoek *et al.*, Nucl. Instrum. Methods A **313**, 377 (1992).
[47] F. Angelini, R. Bellazzini, A. Brez *et al.*, Nucl. Instrum. Methods A **336**, 106 (1993).
[48] R. Bouclier, G. Million, L. Ropelavski *et al.*, Nucl. Instrum. Methods A **332**, 100 (1993).
[49] F. Angelini, R. Bellazzini, A. Brez *et al.*, Nucl. Instrum. Methods A **315**, 21 (1992).
[50] M. Bedjidian, D. Contardo, I. Evangelov *et al.*, Nucl. Phys. B (Proc. Suppl.) **32**, 189 (1993).
[51] C. J. S. Damerell, Preprint RAL-94-096, Rutherford Appleton Laboratory, Daresbury (1994).
[52] C. J. S. Damerell, F. J. M. Farley, A. R. Gillman *et al.*, Nucl. Instrum. Methods A **185**, 33 (1981).
[53] L. M. Soroko, Fiz. Élem. Chastits At. Yadra **10**, 1038 (1979) [Sov. J. Part. Nucl. **10**, 412 (1979)].
[54] C. J. S. Damerell, R. L. English, A. R. Gillman *et al.*, Nucl. Instrum. Methods A **275**, 484 (1989).
[55] P. F. Manfredi and F. Ragusa, Nucl. Instrum. Methods A **252**, 208 (1986).
[56] M. Bacciolini, A. Conti, D. Caporiacco *et al.*, Nucl. Instrum. Methods A **240**, 36 (1985).
[57] M. G. Strauss, Preprint SLAC-PUB-6686, SLAC, Stanford (1994).
[58] E. H. M. Heijne and P. Jarron, Nucl. Instrum. Methods A **275**, 467 (1989).
[59] B. Dierickx, Nucl. Instrum. Methods A **275**, 542 (1989).
[60] S. Parker, Nucl. Instrum. Methods A **275**, 494 (1989).
[61] G. Hall, Preprint IC/HEP/94-9, Blackett Laboratory, London (1994).
[62] E. H. M. Heijne, F. Antinori, R. Arnold *et al.*, Nucl. Instrum. Methods A **349**, 138 (1994).
[63] C. Kenney, S. Parker, W. Snoeys *et al.*, Nucl. Instrum. Methods A **326**, 144 (1993); C. Kenney and S. Parker, Nucl. Phys. B (Proc. Suppl.) **32**, 460 (1993).
[64] G. T. Reynholds and P. E. Condon, Rev. Sci. Instrum. **28**, 1098 (1957).
[65] J. Kirby, Preprint CERN-EP/87-60, CERN, Geneva (1987).
[66] A. Simon, Preprint CERN/PPE 92-95, CERN, Geneva (1992).
[67] C. Angelini, W. Beusch, A. Cardini *et al.*, Preprint CERN-EP/89-120, CERN, Geneva (1989).
[68] C. Angelini, W. Beusch, A. Cardini *et al.*, Preprint CERN-EP/89-112, CERN, Geneva (1989).
[69] C. Angelini, W. Beusch, A. Cardini *et al.*, Nucl. Instrum. Methods A **289**, 342 (1990).
[70] C. Fisher, Nucl. Instrum. Methods A **263**, 159 (1988).
[71] C. Angelini, W. Beusch, and I. J. Bloodworth, Nucl. Instrum. Methods A **277**, 132 (1989).
[72] C. Angelini, W. Beusch, A. Cardini *et al.*, Nucl. Instrum. Methods A **289**, 342 (1990).
[73] C. Angelini, W. Beusch, A. Cardini *et al.*, Nucl. Instrum. Methods A **289**, 356 (1990).
[74] M. N. Atkinson, D. J. Crennell, C. M. Fisher *et al.*, Nucl. Instrum. Methods A **263**, 333 (1988).
[75] M. Salomon, H. Coombes, M. Nissen *et al.*, IEEE Trans. Nucl. Sci. **NS-34**, 525 (1987).
[76] J. Bahr, K. Hiller *et al.*, Preprint 93-201, DESY, Zeuthen (1993).

[77] V. Agoritas, N. N. Akchurin, A. M. Bergdolt *et al.*, Preprint CERN-PPE/94-126, CERN, Geneva (1994).
[78] M. Atkinson, D. Crennell, C. M. Fisher *et al.*, Nucl. Instrum. Methods A **237**, 505 (1985).
[79] F. Takasaki, H. Saito, T. Shimizu *et al.*, Nucl. Instrum. Methods A **262**, 224 (1987).
[80] J. G. Timothi, IEEE Trans. Nucl. Sci. **NS-32**, 427 (1985).

Translated by Patricia A. Millard